Advanced Fiber Materials (2023) 5:429–460
https://doi.org/10.1007/s42765-022-00237-5

REVIEW

A Review on Electrospinning as Versatile Supports for Diverse Nanofibers and Their Applications in Environmental Sensing

Jialing Song[1,3] · Xuanhao Lin[3] · Liang Ying Ee[3] · Sam Fong Yau Li[3,5] · Manhong Huang[1,2,4]

Received: 19 August 2022 / Accepted: 13 November 2022 / Published online: 5 December 2022

Abstract

Rapid industrialization is accompanied by the deterioration of the natural environment. The deepening crisis associated with the ecological environment has garnered widespread attention toward strengthening environmental monitoring and protection. Environmental sensors are one of the key technologies for environmental monitoring, ultimately enabling environmental protection. In recent decades, micro/nanomaterials have been widely studied and applied in environmental sensing owing to their unique dimensional properties. Electrospinning has been developed and adopted as a facile, quick, and effective technology to produce continuous micro- and nanofiber materials. The technology has advanced rapidly and become one of the hotspots in the field of nanomaterials research. Environmental sensors made from electrospun nanofibers possess many advantages, such as having a porous structure and high specific surface area, which effectively improve their performance in environmental sensing. Furthermore, by introducing functional nanomaterials (carbon nanotubes, metal oxides, conjugated polymers, etc.) into electrospun fibers, synergistic effects between different materials can be utilized to improve the catalytic activity and sensitivity of the sensors. In this review, we aimed to outline the progress of research over the past decade on electrospinning nanofibers with different morphologies and functional characteristics in environmental sensors.

Keywords Electrospinning · Nanofibers · Environmental sensing · Functional nanomaterials

Introduction

Rapid global industrialization and urbanization not only have resulted in significant economic benefits, but also led to resource depletion and grave environmental pollution problems, including air, soil, water, and energy (light, sound, heat, and radioactivity) pollution [1]. The large amounts of flammable, toxic, and harmful gases emitted from intensive industrial production and urbanization exacerbate air pollution. Motor vehicle emissions, comprising a large amount of greenhouse gases, toxic nitrogen oxide, sulfur oxide, and other gases, are one of the leading reasons for air pollution [2, 3]. Many indoor decoration materials are not environmentally-friendly and produce large amounts of carcinogenic formaldehyde, toluene, and other volatile solvent vapors. These gaseous pollutants not only cause global warming, haze, acid rain, and other environmental pollution problems, but also acutely jeopardize human health [3]. In the aquatic environment, pollution is aggravated by a large amount of improperly discharged wastewater, including wastewater contaminated by antibiotics from pharmaceutical companies and livestock farms, heavy metals from industrial manufacturing processes, and pesticides from agriculture and horticulture. Numerous harmful pollutants in the aquatic environment can easily enter the human body through several pathways, especially through the food chain where they can cause different food-borne diseases and even the formation

✉ Manhong Huang
huangmanhong@dhu.edu.cn

1 College of Environmental Science and Engineering, Key Laboratory of Science and Technology of Eco-Textile, Ministry of Education, Donghua University, Shanghai 201620, People's Republic of China

2 Shanghai Institute of Pollution Control and Ecological Security, Shanghai 200092, People's Republic of China

3 Department of Chemistry, National University of Singapore, 3 Science Drive 3, Singapore 117543, Singapore

4 State Key Laboratory for Modification of Chemical Fibers and Polymer Materials, Donghua University, Shanghai 201620, People's Republic of China

5 National University of Singapore Environmental Research Institute, T Lab Bldg, 5A Engineering Drive 1, Singapore 117411, Singapore

of "super bacteria" [4–6]. Agricultural pollutants, and their by-products produced in soil, can cause serious damage to human health after entering the food chain. Among the many food safety problems caused by soil pollution, contamination by heavy metals, such as Pb, As, Cr, and Hg, is the most serious. Therefore, the development of sensor technologies with superior performance metrics, such as high sensitivity, rapid response, and good selectivity and stability, is crucial; however, it remains a major challenge. Recently, there has been increasing interest in the use of chemical sensors for the analysis of environmental contaminants. Owing to the benefits of easy sample preparation, miniaturization, portability, and the low cost of producing the new chemical sensors, these sensors can complement or even replace classical analytical instruments in real-time on-site or online detection [7–10].

The type and structure of the sensing material are pivotal to the performance of the chemical sensing technology. Previously, a strategy has been proposed to improve the performance of a sensor by enhancing the transfer capability between the sensing material and the target analytes by adjusting the specific surface area of the sensing material [11]. In this context, nanomaterials play an important role in the field of sensor technology owing to their unique dimensional properties. Furthermore, sensors fabricated using diverse nanomaterials with tunable sizes and surface functional groups have been reported to remarkably increase sensitivity and expand the range of target contaminants. Nanomaterials are widely recognized for their excellent prospects in the development of advanced sensing technologies [11]. By adapting and optimizing electrospinning, nanofibers with unique structures, morphologies, and functions can be produced. Therefore, electrospinning technology has been recognized as a highly promising method in the design and development of nanomaterial-based ultra-sensitive sensor systems [12–14].

During electrospinning, a polymer solution or melt is charged and deformed by a high-voltage electrostatic field, forming a pendant cone-shaped droplet at the end of a nozzle [13, 15]. When the charge repulsion on the surface of the droplet exceeds its surface tension, tiny jets of the polymer fluid, referred to as "jets", are ejected at a high speed from the surface of the droplet towards the plate electrode at a relatively short distance to form the polymer fibers [16, 17]. When the diameters are scaled down from micron to sub-micron or even nanometer, polymer fibers exhibit several unique properties. Conventional preparation methods for nanofibers include stretching, template synthesis, phase separation, and self-assembly [5, 12, 18, 19]. The diameters of fibers prepared using conventional approaches are in hundreds of microns, whereas those obtained by electrospinning are 2-3 orders of magnitude smaller. The specific surface area of conventional fibers is normally 0.4 $m^2\ g^{-1}$, while that of electrospun fibers is typically 40 $m^2\ g^{-1}$ [18, 19]. Electrospinning substantially increases the surface area-to-volume ratio of the nanomaterials (up to 1,000-fold higher for ultrafine fibers) [13]. Moreover, the mechanical strength, hydrophilicity/hydrophobicity, electrical conductivity, and flexibility of nanomaterials can be tailored as required via polymer selection, concentration modulation, optimization of electrospinning parameters, and chemical modification through functionalization [13, 20, 21]. There are two main approaches for the preparation of sensors by electrospinning. The first approach produces nanofibers with direct sensing functions by electrospinning functional polymers, such as polyacrylic acid and polyacrylonitrile (PAN) and utilizing these nanofibers directly as the sensing elements of the sensors [13, 20]. The second approach uses electrospun nanofibers as stencils and deposits responsive sensing materials with surface functionalization on the fiber surface to create micro- and nanostructures with selective sensing properties [22]. Nanofibers prepared via electrospinning generally exhibit a large specific surface area with most atoms located on the surface or within interfacial regions, exhibiting high chemical reactivity owing to their unique and complex surface structure [20]. One-dimensional nanomaterials prepared via electrospinning are not limited to nanometer size and can have a high aspect ratio for the fast transfer of electrons [13, 14]. Therefore, the introduction of nanomaterials with a high specific surface area during the design of sensing materials favors both sensitivity enhancement and response time reduction.

Compared with the hydrothermal and templating methods, the electrospinning technology is more flexible for nanomaterial preparation. It can regulate the morphology, structure, composition, and function of the nanofibers in a diverse and multifaceted manner via polymer concentration, co-blending of different polymers, and chemical cross-linking between polymers [14, 20]. The electrospinning technology enables the continuous preparation of nanomaterials with different structures and morphologies, including nanofibers, nanowires (nanorods), nanoribbons, hollow nanofibers, core-shell structures, hollow nanotubes, nanodendrites, etc. [22–30]. In addition, nanomaterials prepared via electrospinning exhibit high axial strength and can achieve continuous electron transfer, which facilitates charge transfer along the long-axis direction and enables higher sensitivity for sensors fabricated in this way [13, 15, 31]. Electrospinning is facile, and the derived materials are highly reproducible and scalable for industrial production. Owing to these characteristics, the electrospun nanofibers provide greater selectivity towards environmental sensing.

In this review, we sought to provide an overview of the applications of electrospinning in the field of environmental sensing over the past decade. This review further discusses progress from multiple perspectives on environmental

sensing by comparing and summarizing the morphology, function, and composition of nanomaterials prepared using the electrospinning technology.

Electrospinning and Nanofibers

Background

Electrospinning is a technology in which polymer solutions are sprayed and stretched under the action of static electricity to obtain nanoscale fibers. The electrospinning equipment is mainly composed of three parts: a high-voltage power supply, micro-injection pump and nozzle, and fiber-receiving substrate. A high-voltage direct current (several thousands to tens of thousands volts) is applied to the polymer solution. When the electric field force is sufficiently large, the charged polymer droplets overcome the surface tension to form a jet stream that evaporates or solidifies with the solvent during the jetting process [13, 32]. Finally, it falls on the collection substrate to form a fiber mat that is similar to a non-woven fabric. The diameters of the nanofibers formed range between tens of nanometers (nm) and micrometers (μm). Generally, the fiber membranes collected on the collector substrate are composed of randomly oriented and entangled fibers. With a specially designed collector substrate, fibers with high strength and toughness can be obtained in highly aligned patterns. Special collectors (Fig. 1), such as high-speed rotating drum collectors, parallel collectors, and tip collectors, are suitable for obtaining aligned fibers [16, 33, 34].

Traditional electrospinning equipment commonly adopts a single capillary nozzle and is generally employed to prepare solid and smooth nanofibers. However, only nanofibers composed of a single material can be obtained from the traditional equipment, and hence accompanied with several shortcomings that include insufficient surface specificity and poor mechanical properties. It is difficult to prepare composite materials with multiple functional structures. Although these materials can be adopted for a wide

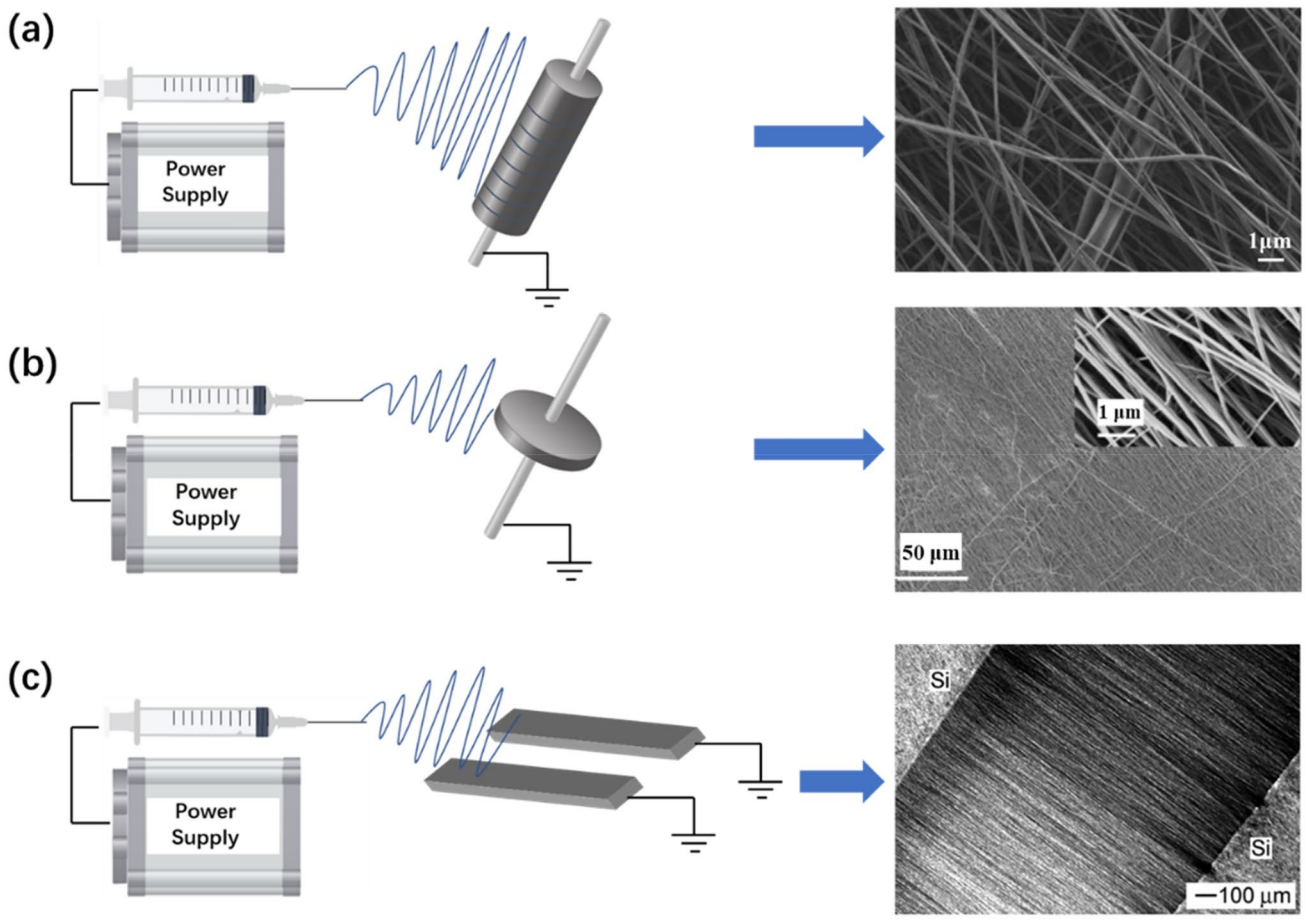

Fig. 1 Special collectors for obtaining aligned fibers: **a** high-speed rotating drum collectors; reproduced with permission from ref. [16], Copyright 2018, Elsevier. **b** Tip collectors; reproduced with permission from ref. [33], Copyright 2003, American Chemical Society. **c** Parallel plates collectors; reproduced with permission from ref. [34], Copyright 2010, Elsevier

range of applications [12, 35]. To overcome these shortcomings, researchers have improved electrospinning via three strategies: (1) surface modification of nanofibrous membranes, (2) blending multiple functional materials, and (3) coaxial electrospinning technique. These strategies proved convenience in preparing continuous core-shell nanofibers or hollow-structured nanofibers in a single step. In the coaxial electrospinning process, mixing does not occur before solidification due to the short confluence time and low diffusion coefficient of the two spinning solutions at the capillary outlet. When a high-voltage electric field is applied to the liquids in the inner and outer orifices of the capillary, the charges of the solution in the inner orifice gradually migrate to the solution surface in the outer orifice [32]. Increase in voltage, and electric field, results in a gradual increase in the amount of charge on the solution surface in the outer orifice [12, 36]. When the charge reaches a certain limit, its repulsive force causes the outer solution to form a composite Taylor cone at the electrospinning nozzle followed by a coaxial composite structure with a core-shell double layer. A hollow nanofiber is formed when the core (inner) layer is removed through heating or dissolution in suitable solvent system.

Key Regulating Factors in the Electrospinning Process

Characteristics of the Electrospinning Solution

Polymer: Electrospinning has been recognized as a low-cost, convenient, and environmentally friendly method that is widely adopted to produce nanofibers with various morphologies and functions [12]. Water-soluble polymers, such as poly (vinylpyrrolidone), polyethylene oxide, poly (vinyl acetate), and polyvinyl alcohol (PVA), and solvent-soluble polymers, such as polyimide, PAN, polyvinylidene fluoride (PVDF), poly (methyl methacrylate), and polystyrene (PS) are the most common polymers used in electrospun nanofibers. Notably, the addition of multifunctional materials, such as metal oxides, inorganic non-metals, metal–organic frameworks, and covalent organic frameworks, to polymers allows the preparation of composite nanofibers with different morphologies, structures, and functionalities under controlled conditions [37–39].

Conductivity: The conductivity of the electrospinning solution is another key parameter that affects the morphology of electrospun fibers and contributes to jet formation. The addition of salts, ionic polymers, or conductive polymers to the electrospinning solution increases the solution conductivity and supports the formation of high-quality fibers with fewer defects and smaller diameters [40].

Surface Tension: In electrospinning, a trickle is ejected when the charged solution overcomes its surface tension. Generally, high surface tension in a liquid reduces its surface area, maintains its spherical shape, and is the predominant contributing factor towards the formation of liquid beads [40]. Therefore, the surface tension of the electrospinning solution is minimized to enlarge its surface area as much as possible to prevent the formation of liquid beads and reduce the fiber diameter. Routine approaches to reduce the surface tension of the solution include (1) the use of a solvent with low surface tension, such as ethanol or acetone, and (2) the addition of surfactants into the electrospinning solution.

Concentration and Viscosity of the Electrospinning Solution: Low polymer concentration typically results in low viscosity that causes the jet to be unstable and discontinuous. Such a low concentration also results in the formation of beaded nanofibers in which this phenomenon is known as the "flying filaments". Viscosity increases with increasing polymer concentration [41]. However, the flow of the solution is hindered when the polymer concentration exceeds a certain limit, causing nozzle blockage or what some authors refer to as "non-spinning" [13].

Equipment Parameters

Electric Field Intensity: Low voltage applied cannot overcome the surface tension of the electrospinning solution due to a low electric field, which hinders the stretching and splitting of the solution, resulting in larger nanofiber diameters [35]. As the electric field strength increases, higher surface charge density and electrostatic repulsion accumulate on the jet of the polymeric electrospinning solution. Simultaneously, a higher electric field strength accelerates the jet to a higher velocity. These factors contribute to the formation of fibers with greater tensile stress and finer textures. However, a high electric field strength over a certain limit induces a very fast jet flow and hampers its stretching and splitting, which consequently results in larger fiber diameters, worse uniformity, and beaded fibers [42–44].

Needle Pitch: The distance between the electrospinning needle and collector affects the electric field strength and volatilization of the electrospinning solution, thereby altering the diameter of the nanofibers. When the voltage is kept constant, the electric field strength is inversely proportional to the distance. In a typical electrospinning setup, the distance ranges from 10 to 15 cm, which usually allows sufficient evaporation of the solvent from the jet before being deposited as a dried fiber bundle. If the distance is too short to allow sufficient evaporation of the solvent of the jet, unfavorable fused fibers may be formed [44, 45].

Flow Rate: The electrospinning rate is controlled by the flow rate of the syringe. The electrospinning rate not only governs the production of high-quality nanofibers, but more importantly influences the jet stability and fiber diameter,

which increases with decreasing electrospinning speed [32, 46].

Environmental Factors

Environmental temperature and humidity in the electrospinning process have a significant impact on the evaporation rate of jet solvents and the morphology and diameter of the produced fibers. Temperature is known to affect solvent evaporation, Brownian motion, and the diffusion of ions, atoms, molecules, and particles. The increased temperature of the electrospinning solution reduces its viscosity and elevates its solvent evaporation and Brownian motion, ultimately altering the fiber diameter [47]. Humidity also changes the volatilization rate of solvents in the spinning solution, affecting the void distribution on the surface of the electrospun nanofibers. Several studies have revealed a relatively smoother surface of electrospun fibers produced with less than 25% humidity and a rougher surface with more pores on the fiber surface as humidity exceeds 30%. Notably, very low humidity speeds up the solvent evaporation of a jet and increases its viscosity, both of which may cause nozzle clogging at the capillary tip. In contrast, high humidity aggravates the formation of dangerous conducting air and slows solvent volatilization [38, 48].

Diversity of the Fiber Structure

The structure of electrospun fibers is one of the factors governing their performance. Fibers fabricated using multiple electrospinning techniques produce different types of structures and morphologies than those using a single type of electrospinning. Fibers with unique structures, morphologies, and functions can be produced by selecting and optimizing the suitable type of electrospinning technique.

Individual Single Types of Electrospinning

Beaded Fiber: Beaded fibers are formed by unstable fluid jets under an external electric field. Owing to their unique structure, they can be applied in different applications. Moreover, it has become possible to carry out the corresponding theoretical modelling on the formation of beaded fibers with the rapid advancement in electrospinning technology in the recent years [30, 49, 50].

Core-Shell/Hollow Nanofiber: Electrospun core-shell/hollow nanofibers have been widely assessed and applied by many researchers in sensing systems. These nanofibers can be produced by coaxial or emulsion electrospinning. In the former process, the outer and inner electrospinning solutions are delivered to two capillaries with different inner diameters. Thereafter, they combine to form a coaxial Taylor cone followed by coaxial fluid jets in a high-voltage electrostatic field, of which the jets solidify into core-shell nanofibers with different interior and exterior contents. If the core layer is removed via heating or dissolution, hollow nanofibers are formed with a hollow inner lumen surrounded by an intact outer layer.

Prior studies revealed that polymeric electrolytes based on ionic liquids do not only have high conductivity, but also excellent mechanical properties [51–53]. Ionic gels with high capacitance can be used as thin films to prepare capacitive sensors [54]. However, the surface of a hydrogel (ionic gel) is prone to dehydration. Therefore, a protective mechanism must be developed to prevent water from evaporating from its surface [55]. In addition, surface area affects the capacitance of an ionic hydrogel matrix film and limits the sensitivity and stability of its capacitive sensor device. Lin et al. [29] overcame the above-mentioned problems using the coaxial electrospinning method. An ionic gel was employed as the core with the copolymer PVDF as the outer shell to produce a core-shell nanofiber mat. The advantages of a co-polymer shell include its larger surface area and sealed protective layer that effectively prevents dehydration of the core-shell ionic gel.

Liu et al. [56] developed a chemical sensor based on the core-shell structured semiconductor nanofibers through rapid single-nozzle electrospinning process and spontaneous phase separation. The rich active sites of the core-shell structured nanofibers effectively promote interactions between charge carriers in their conductive channels and chemical analytes, and change the output current and charge carrier mobility that lead to a high sensitivity in the resulting sensor. The shell thickness in a core-shell structure can be adjusted by changing the ratio of the outer and inner electrospinning solutions in the mixed solution. A nanofiber-based sensor with an appropriate core-shell ratio exhibits high sensitivity toward low concentrations of ammonia (the limit of detection was as low as 50 ppb).

Hollow nanofibers with porous surfaces and tubular structures also exhibit outstanding properties. Electric current can easily flow around their disturbance zone and target contaminants can freely diffuse in and out of them, thereby shortening the response and recovery time [57]. Park et al. [28] took advantage of the Kirkendall effect to fabricate porous hollow nanofibers of SnO_2-CuO nanocomposite by single-needle electrospinning. The Kirkendall effect arises from the supersaturation of lattice vacancies caused by the different diffusivities of distinct atoms. A nanotube structure is formed after calcination, which is attributed to the Kirkendall effect [58]. A fast response was achieved with the prepared SnO_2-CuO hollow nanofiber-felt for the detection of H_2S gas with a rapid detection time of 5.27 s and a low concentration range of 1–40 ppm.

Porous Fiber: Emerging porous materials generally have channels, pores, and gaps on their surfaces or interiors.

These materials also usually have the characteristics of low density, high specific surface area, high porosity, and high adsorption capacity and thus widely adopted in sensors, filtration, catalysis, and other applications [59–61] reported that the calcination of electrospun PVA composite nanofibers containing silica sol nanoparticles at 450 °C produced porous inorganic nanofibers with high specific surface areas. Liu et al. [62] prepared porous alumina nanofibers with hollow structures by sintering aluminum-nitrate/PAN nanofibers through high-temperature calcination. Ma et al. [63] prepared the porous PAN nanofibers by washing electrospun PAN/$NaHCO_3$ composite nanofibers with a 10% hydrochloric acid solution to dissolve and remove $NaHCO_3$, and the escaping CO_2 gas "blown" nanopores in the PAN nanofibers. The electrospun porous nanofibers also had discontinuous pore structures in the interior or open pore structures on the surface. The porous structure of nanofiber materials provides superior properties, including large specific surface areas and reduced thermal conductivity, which further broadens their application range.

Others: Electrospinning can be employed to generate fibers of various shapes, such as beaded, core-shell, ribbon, porous, spiral, square, and honeycomb (Fig. 2). Zhang et al. [22] prepared membranes with electrospun ribbon nanofibers and suggested that the formation of a fiber-ribbon shape could be attributed to the positive charge of the polymer precursor. According to the study, a jet carrying negative charge on its surface attracts the positively charged polymer precursor to its surface during the electrospinning process, leaving its center solvent-rich and forming a tube-shaped structure with a thin outer layer. When the residual solvent in the tube center evaporated, a partially collapsed hollow tube was formed with wrinkles on the surface. When the hollow tube collapsed completely, a ribbon-like structure was formed. Shin et al. [26] reported a facile process for producing electrospun spiral nanofibers with a single polymer and demonstrated the transformation of nanofibers from spiral to linearly oriented with an adjustment in electric field strength.

Aggregate Electrospinning Structure

Figure 2g–j shows the great diversity in the structures and morphologies of electrospun fiber membranes. The structural diversity mainly depends on the collector type, which is one of the most important parts of the electrospinning equipment and determines the distribution and macrostructure of the electrospun fibers. Other aspects of the processing equipment, such as the electric field strength, presence of a magnetic field, and composition of the electrospinning solution, can be optimized to obtain the desired fiber mat structures. The collected electrospun fibers or fiber mats are generally divided into three groups: random fibers, arranged fibers, and pattern fibers.

Random Electrospinning: Random fibers are the most common form of electrospun fiber collection. Randomly oriented fibers can be obtained simply using a traditional electrospinning collector. Charged polymer jets naturally travel along spiral trajectories during the electrospinning process and finally solidify into randomly oriented continuous fine fibers on a ground plate substrate.

Oriented Electrospinning: Regularly oriented electrospun nanofibers can be prepared using a special collector and electrodes. Park et al. [25] prepared a hybrid scaffold with a dual configuration of aligned and random electrospun fibers. Wang et al. [62] prepared ordered parallel arrays of PVA nanofibers using similar hybrid scaffolds and successfully applied them to the detection of low concentrations of NO_2.

Patterned Electrospinning: Patterned electrospun nanofibers can be produced using appropriate solutions and a special collecting device. Liang et al. [24] prepared an oriented square microfiber mat using an electrostatic template for nanofibers deposition on a pattern collector made of regularly distributed protrusions. Gangolphe et al. [23] developed honeycomb electrospun scaffolds and successfully applied them to prepare honeycomb fibrous membranes with appropriate macropore size and fiber arrangement. These researchers also assessed the anisotropic and mechanical properties, and the degradation mechanism of honeycomb membranes.

Application of Electrospinning in Environmental Sensing

Electrospun sensing and interface materials have gradually been adopted in the construction of various sensors, mainly using the following characteristics: (1) nanofibrous membrane materials used as sensors with a range of specific surface areas that can be obtained by adjusting the fiber geometry and pore size; (2) the specificity and diversity of fiber materials offer different characteristics and a wide range of applications; (3) the strong molecular recognition ability of electrospun sensors eliminates tedious sample pre-treatment, and their reusability leads to simple and rapid detection processes; (4) the sensor interface has high sensitivity and quick response to a small quantity of samples; (5) electrospun sensors have good repeatability, stability, and reusability; and (6) their detection cost is low. More specifically, the high surface area of electrospun nanofibers offers more active adsorption sites for target analytes to be adsorbed on the sensing interfaces. In addition, the adsorption and desorption rates of electrospun nanofibers are significantly accelerated for rapid sensing and improved sensitivity [64]. According to prior studies, the enhanced sensing rate can be attributed to the high surface-area-to-volume ratio [65]. The Debye lengths of the nanofibers, which refers to the distance over

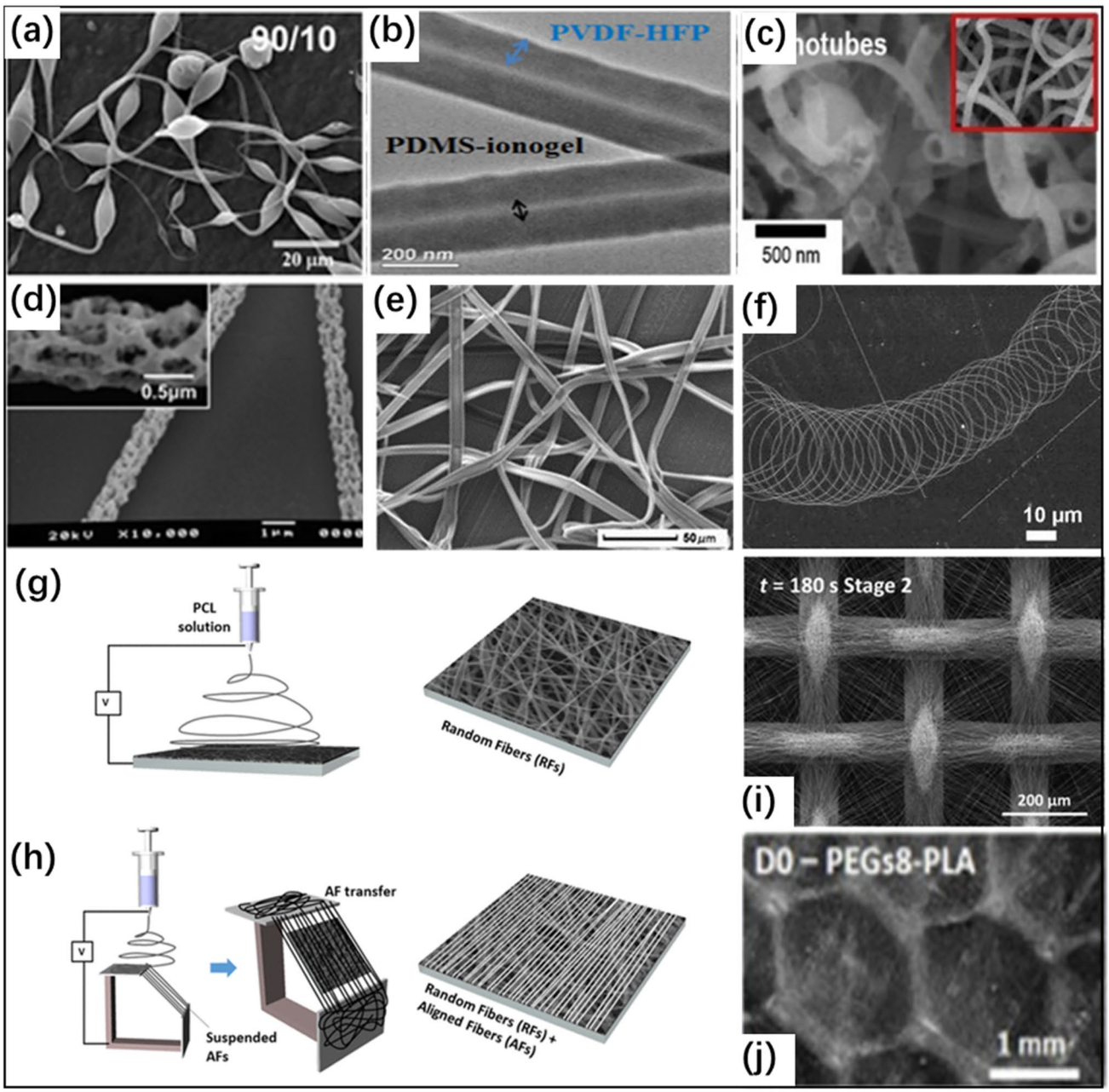

Fig. 2 Various morphologies of electrospun fibers: **a** beaded fibers; reproduced with permission from ref. [30], Copyright 2015, Wiley. **b** Core-shell fibers; reproduced with permission from ref. [29], Copyright 2018, Elsevier. **c** Hollow fibers; reproduced with permission from ref. [28], Copyright 2020, Elsevier. **d** Porous fibers; reproduced with permission from ref. [27], Copyright 2008, American Chemical Society. **e** Ribbon fibers; reproduced with permission from ref. [22], Copyright 2019, Wiley. **f** Spiral fibers; reproduced with permission from ref. [26], Copyright 2006, American Institute of Physics. **g** Random fibers and **h** aligned fibers; reproduced with permission from ref. [25], Copyright 2016, American Chemical Society. **i** Square-patterned fibers; reproduced with permission from ref. [24], Copyright 2021, Wiley. **j** Honeycomb-patterned fibers; reproduced with permission from ref. [23], Copyright 2021, Elsevier

which significant charge separation can occur, are equivalent to their diameters. Charge accumulation/consumption areas, where the adsorption of analyte molecules occurs, extend from their surface into their interior and seriously affect current flow. Compared with two-dimensional thin films, the current in 1D nanofibers can still flow easily around the disturbed area [28, 57]. Therefore, their response is fast and the recovery time is short when the target molecules quickly diffuse into the sensing material. In addition to polymers, several other functional materials such as metals and organic/inorganic materials can be included into the

electrospinning solutions to prepare multifunctional electrospun nanofibers in sensors.

Gas Sensor

With accelerated industrialization, the global air pollution problem has become increasingly serious. Air pollutants contain different toxic gases, such as CO, SO_2, NO_2, and H_2S, and volatile organic compounds (VOCs), such as benzene, toluene, and formaldehyde. These hazards can cause respiratory system damage, physiological dysfunction, digestive system disorders, nervous system abnormalities, mental decline, carcinogenesis, and disability. High concentrations of air pollutants can cause acute poisoning or even diseases [66–68]. According to the "2019 Global State of the Air" report recently released by the US Institute of Health Effects (based on 2017 data), the number of people who died of stroke, heart disease, lung cancer, diabetes, and chronic lung disease worldwide due to air pollution reached nearly 5 million in 2017. Notably, severe air pollution can even cause abnormalities in the components of pulmonary surfactants or even lung damage, making humans more susceptible to diseases, including COVID-19 [69]. Air pollution has become an urgent global problem, and authorities in countries and organizations have specified short-term exposure limits (STEL) for various toxic gases and VOCs [70, 71]. Environmental protection first requires the establishment of an environmental supervision mechanism; gas sensors, as one of the essential sensors for environmental supervision, help the set-up of an environmental Internet of Things [72]. Air quality affects our daily lives, and effective actions must be taken to ensure good air quality. Continuous monitoring of pollutant gases in the air through gas sensors can effectively identify the potential risks of air pollution to human health. Over the past 5 years, many gas sensors with excellent sensitivity, stability, reversibility, response time, and reproducibility have been reported. These gas sensors include resistive gas sensors, quartz crystal microbalance (QCM) gas sensors, and optical sensors with electrospun nanostructured layers composed of polymers and functional TiO_2, SnO_2, ZnO, In_2O_3, Fe_2O_3, WO_3, or other metal oxides [73–75]. In the following sections, we aimed to outline the recent progress and development in this emerging field and highlight the sensing layer microstructures and gas-sensitive properties of electrospun gas sensors.

Resistive Gas Sensor

Compared with traditional gas detection equipment, portable and inexpensive gas sensors have outstanding advantages in terms of shorter detection times, without sacrificing detection accuracy. Resistive gas sensors are one of the most common types of gas detection sensors [76–79]. A resistive sensor is based on changes in the electrical resistance or conductivity caused by the adsorption of gas molecules. Therefore, the response rate depends on the interaction speed and strength between the target gas molecules and the sensor material surface, and the specific surface area available for adsorption and desorption [80]. In an oxygen-rich environment, oxygen molecules adsorbed onto sensor surfaces extract electrons from the conduction band and trap them as negatively charged ions on the surface, forming different surface energy levels. Accordingly, an electron depletion layer and a hole accumulation layer are formed on the sensor surface for the n- and p-type materials, respectively. When switched to a target gas-rich environment, the target gas molecules are adsorbed onto the sensor surface and exchange electrons with it, causing a conductivity change in the sensing material. The resistance/conductivity of gas sensors depends on the charge transfer mechanism between the adsorbed gas molecules and gas-sensitive adsorbents, as well as their surface reactions. When an n-type sensing material is exposed to oxidizing gas, its resistance increases, whereas exposure to reducing gas decreases its resistance [81, 82]. Figure 3 shows the principle of the gas-sensing mechanism of a resistive gas sensor based on the n-type and p-type sensing materials [83].

According to the configuration, resistance gas sensors can be further divided into ceramic tubular, flat, and flexible sensors. The structure and physical diagrams of various resistance gas sensors are shown in Fig. 4. For a long time, the ceramic tubular sensor was the main type owing to its simple preparation process and low cost [85, 86]. As shown in Fig. 4a, the ceramic tube is composed of four parts: ceramic tube, Ni-Cr heater, Au electrode, and Pt wire. The heater is placed in a ceramic tube to maintain the working temperature. Two rings of gold electrodes are placed on the outer wall of the ceramic tube, on top of which is the deposited sensing material for electrical signal production.

When the sensing interface of the gas sensor is porous, the target gas molecules can penetrate the entire sensing layer, thereby improving sensitivity. In addition, a large specific surface area facilitates the interaction between the gas molecules and the sensing material. Commonly used chemical solution deposition technology and ceramic slurry sintering technology for preparing gas-sensitive materials can hardly meet the requirements of porosity and large specific surface area at the same time. However, it is difficult to uniformly coat gas-sensitive materials onto the ceramic tube surface using traditional techniques. Hence, they easily aggregate, their pore sizes are not uniform, and gas molecules at their sensing interface cannot be well diffused. In contrast, sensing layers prepared via electrospinning can fulfill the requirements of both high porosity and large specific surface area, and nanofibers have controllable fiber and pore sizes. For different gases, sensor layers with

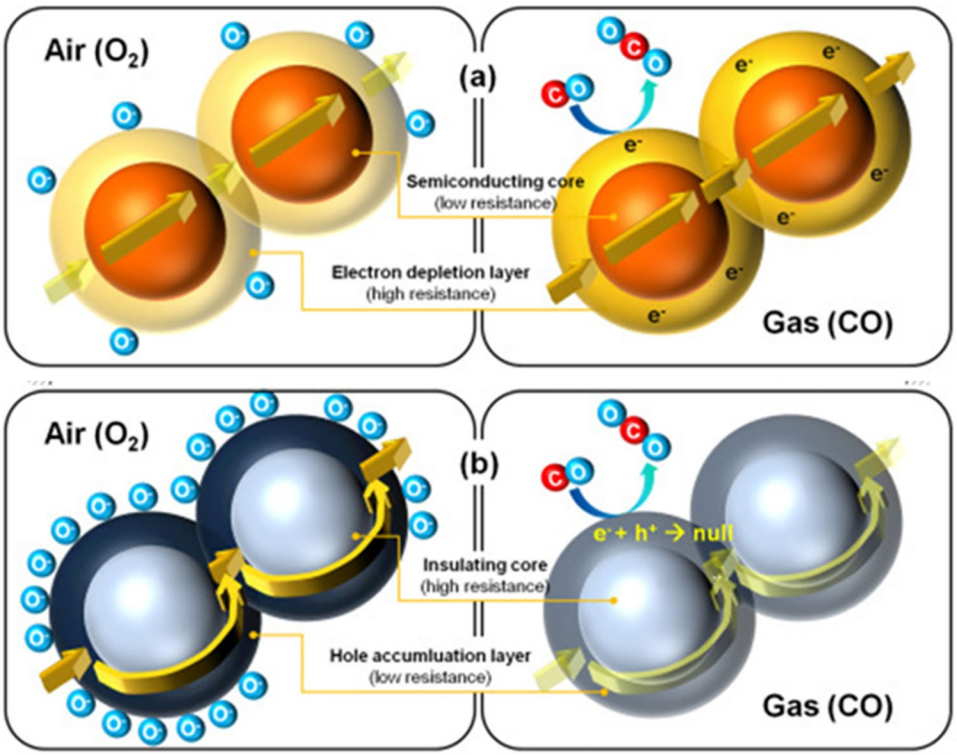

Fig. 3 Schematic illustration of basic sensing principles for **a** n- and **b** p-type MOS gas sensors; reproduced with permission from ref. [84], Copyright 2014, Elsevier

suitable pore sizes can be developed to effectively overcome the gas diffusion limitation, enabling unimpeded penetration of the sensor layer by gas molecules. Han et al. [90] used atomic layer deposition to deposit n-type ZnO on the surface of CuO-polymer hybrid nanofibers. Subsequently, the polymer molecules were removed via calcination to form hollow p-CuO/n-ZnO nanofibers (Fig. 5a, b). The optimal responses of the gas sensor based on the p-CuO/n-ZnO heterostructure were approximately 6- and 45-fold higher than those of pure ZnO and CuO, respectively. Similarly, Zhang et al. [91] reported the use of electrospinning to prepare nanofibers with hierarchical porous heterostructures (p-type Co_3O_4 and n-type In_2O_3). Based on their findings, Co^{2+}/Co^{3+} with high catalytic activity diffused in In_2O_3 with uniform distribution (Fig. 5c). Their results revealed that the gas sensor had a remarkably high response to VOCs, including acetone and formaldehyde. In addition to the heterogeneous structure, the size of the sensing material has a significant impact on its sensitivity. Li et al. [92] successfully prepared electrospun ZnO/$ZnFe_2O_4$/Au nano-mixtures with controllable particle sizes using a combination of electrospinning and atomic layer deposition techniques (Fig. 5d). Their results showed that the response of the prepared ZnO/ZnFe2O4/Au nanocomposite to acetone was 3- and 5.5-fold higher than that of the ZnO/$ZnFe_2O_4$ composites and ZnO, respectively. More interestingly, Zhang et al. [93] synthesized Cr_2O_3-TiO_2 core-shell fibers with different shell thicknesses through a simple coaxial electrospinning technology and discovered that the shell thickness affected the gas sensor performance. As the TiO_2 shell thickness increased, the response characteristics of the prepared core-shell fiber gas sensor to acetone showed a transition from the p-type to n-type. In addition, the formation of a Cr_2O_3-TiO_2 heterojunction in the gas sensor enabled a quicker response to the target gas molecules and a shorter recovery time.

In flat-type sensors, sensing materials are often deposited on the insulating substrate surface of an interdigital electrode (IDE) as shown in Fig. 4b. IDE sensors are favored in the fields of biomedicine and the environment owing to advantages such as miniaturization, low-cost, and large-scale production [94, 95]. Bulemo et al. [96] suggested that gas analytes diffusing into semiconductor metal oxide-based sensing layers require gas-sensing materials to be thin and porous, and exhibit high performance. In their study, hollow SiO_2-SnO_2 core-shell microstrips were prepared by etching away the SiO_2 core with NaOH solution (pH 12) from electrospun calcined highly porous SiO_2-SnO_2 core-shell microstrips (Fig. 6a, b). After sensitizing with platinum nanoparticles (Pt NPs), the prepared hollow nanofibers were used to detect acetone, exhibiting a highly stable response ($R_a/R_g = 93.70 \pm 0.89$) and significant selectivity to as low as 2 ppm acetone in air. Electrospinning has also been employed as an innovative functionalization method for manufacturing polymer nanofibers with a diameter range of 50–500 nm and a nano-network on the movable plate of a capacitive micromachined ultrasonic transducer

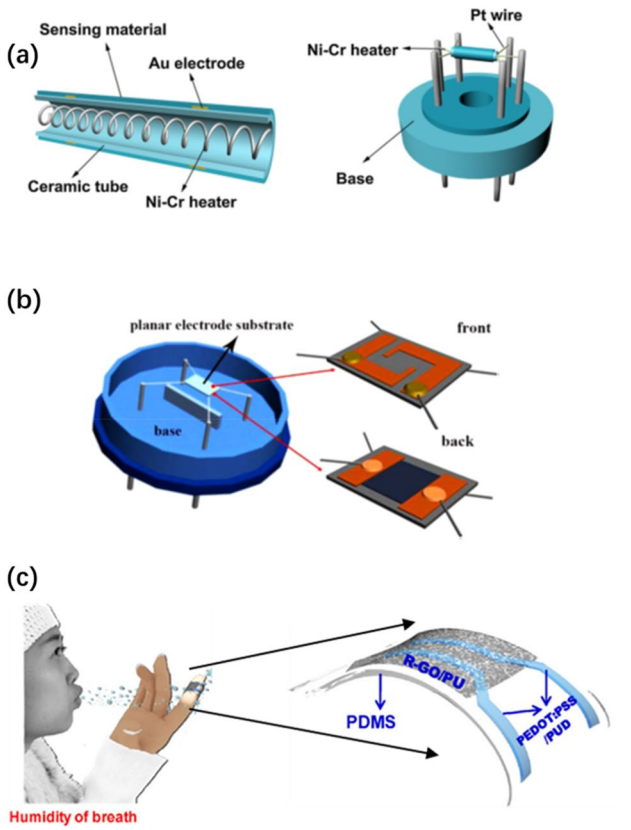

Fig. 4 Schematic and optical images of various resistive gas sensor configurations: **a** tubular; reproduced with permission from ref. [87], Copyright 2020, Elsevier. **b** Plate-like; reproduced with permission from ref. [88], Copyright 2020, Elsevier. **c** Wearable gas sensor; reproduced with permission [89], Copyright 2017, Tsinghua University Press

(CMUT). Zhao et al. [97] reported a CMUT-based resonant biochemical sensor that was prepared to detect SO_2. The resonance frequency shift of this sensor rapidly changed as the SO_2 concentration changed (Fig. 6c, d). Bai et al. [98] synthesized a layered heterostructure composed of thin MoS_2 nanosheets vertically grown on SnO_2 nanotubes through simple electrospinning and hydrothermal strategies (Fig. 6e). This heterojunction expands the surface area of MoS_2@SnO_2, thereby providing more adsorption sites for gas adsorption. The heterostructure formed by the nanofibers facilitated electron communication between MoS_2 and SnO_2, which promoted charge generation and enhanced the charge separation efficiency (Fig. 6f). The prepared sensing interface MoS_2@SnO_2 responded to 34.67–100 ppm NO_2 at room temperature in a time-period as less as 2.2 s.

In recent years, flexible sensors have attracted considerable attention. Flexible gas sensors are key components of portable electronic devices, which have been widely used for on-site environmental and health monitoring owing to their small size, light weight, and strong flexibility [99–101]. Nair et al. [102] fabricated a CNFs@Ni-Pt nanohybrid on a flexible polyester substrate by electrospinning and chemical reduction and tested it with an H_2 sensor (Fig. 7a, b). The integration of bimetallic Ni and Pt nanocatalysts on CNF provides more active sites for hydrogen sorption and improves the hydrogen sensing performance of the sensor. Based on this sensor, the research team achieved a wide range of concentration (0.01–4%) of hydrogen detection. Furthermore, after several bending cycles, a good response to H_2 (50% strength compared with that before bending) was still exhibited owing to the high aspect ratio of the carbon nanofibers. Khalifa and Anandhan [103] developed a gas sensor based on electrospun blend nanocomposite film (EBNC), which was shown in Fig. 7c, d. The EBNC sensor showed good response (approximately 92% saturation with 108 ppm analyte) and high selectivity for NO_2 gas. Furthermore, this sensor was stable for more than 30 days and 100 operation cycles, demonstrating excellent durability. Notably, even after repeated bending cycles, the performance of the sensor did not decrease. This result demonstrates that the electrospun nanofibers were flexible, and their sensing performance was not affected by the bending stress.

Optical Gas Sensor

Although optical sensing technology appeared relatively late, its development is the fastest in gas-sensing technology. Commonly used types in the industry include ultraviolet analyzers, infrared gas analyzers, light scattering analyzers, photoelectric colorimetric analyzers, chemiluminescence analyzers, etc.

Fluorescent probes have been widely explored because of their convenient non-invasive operations [104]. The fluorescence of traditional organic fluorophores is often affected by aggregation-caused quenching (ACQ), hence, the stability of sensors made of them is also seriously affected. Fluorescent agents that exhibit aggregation-induced emission (AIE) characteristics have attracted much attention because they can overcome the ACQ problem [105–107]. In addition, volatile acidic and alkaline gases such as hydrochloric acid and ammonia are common hazardous components in flue gases emitted from industrial production processes. They are usually toxic, harmful, and corrosive, and are extremely detrimental to human health. It was demonstrated that organosilicon precursors with AIE characteristics covalently attached to periodic mesoporous organosilicon (PMO) frameworks had high fluorescence efficiency [108, 109]. Electrospun three-dimensional ordered porous materials provide abundant active sites for gas adsorption/desorption, allowing them to be used for the quick and sensitive monitoring of pollutant gases. Gao et al. [110] prepared a flexible film of dispersed periodic mesoporous organosilicas (PMOs) nanospheres in a mixed fiber matrix (PMO-CFs) by

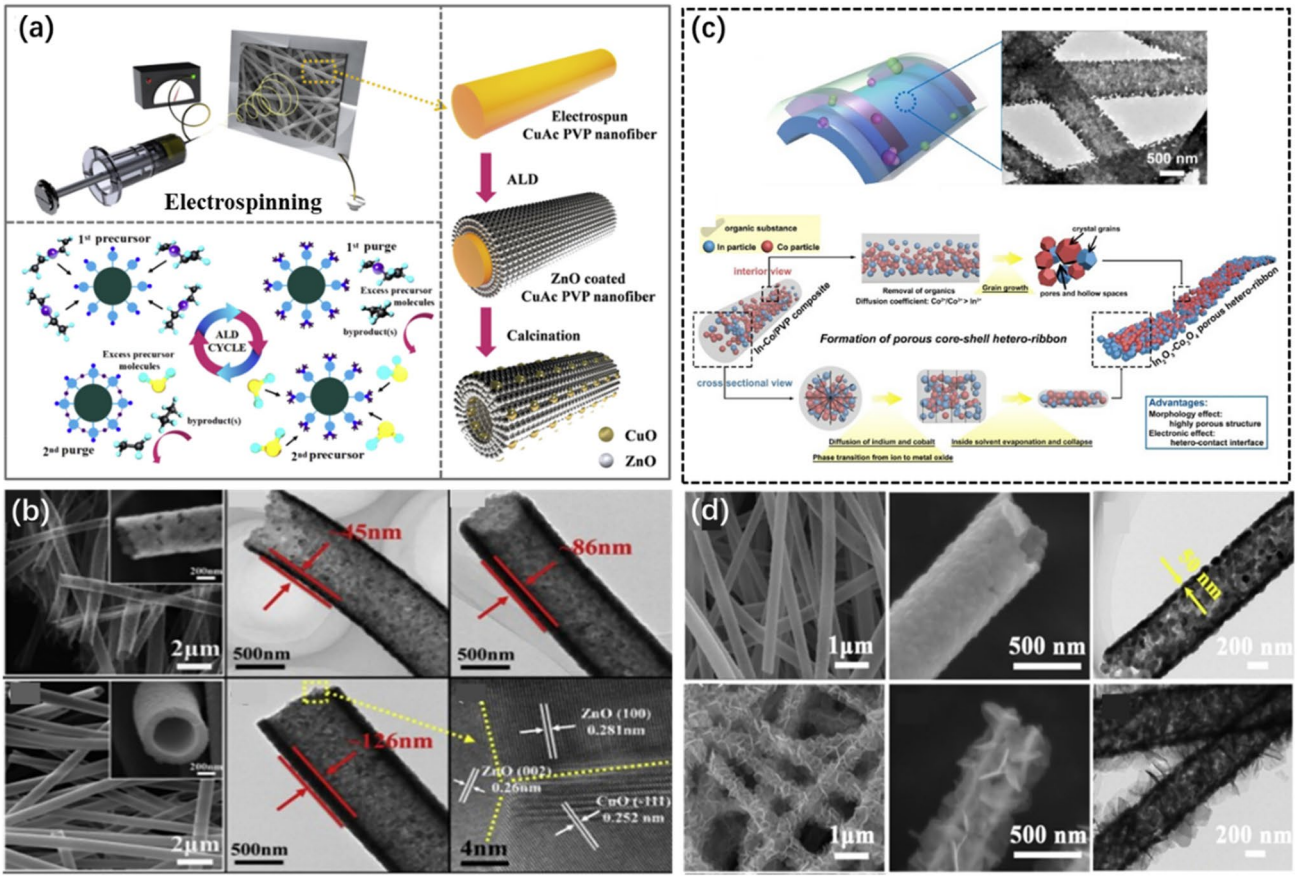

Fig. 5 **a** Schematic illustration of 1D p-CuO/n-ZnO hollow nanofibers synthesis using a three-step method and **b** XRD, SEM, and TEM images of $0.3CuO/ZnO_{200}$, $0.3CuO/ZnO_{400}$ and $0.3CuO/ZnO_{600}$ HNFs; reproduced with permission from ref. [90], Copyright 2019, Elsevier. **c** SEM and XRD pattern of In_2O_3-Co_3O_4 ribbon; reproduced with permission from ref. [91], Copyright 2020, Elsevier. **d** SEM and TEM images of pure ZnO hollow nanomeshes and $ZnO/ZnFe_2O_4$ composites; reproduced with permission from ref. [92], Copyright 2019, Elsevier

electrospinning and assembly technologies and successfully applied it as an efficient fluorescent probe for the detection of ammonia and hydrochloric acid vapor by naked eyes, which was shown in Fig. 8a–c. In addition, the PMO-CF sensor was easy to be regenerated and very stable to light over a long period of time (fluorescence still above 94% after 10 cycles of regeneration).

Polymers that have been utilized in optical oxygen sensors thus far include polystyrene, hydrogel, silicone rubber, various copolymers, and fluorinated polymers [112–114]. The inclusion of fluorine can increase the rate of diffusion of oxygen molecules in fluorinated copolymers [115], which promotes the sensor to have higher sensitivity owing to the high quenching efficiency [114]. Polymer microfibers, notably fluorocopolymer fibers, are promising functional materials for optoelectronic devices, sensing, and energy storage due to their different surface properties [116, 117]. However, the existing fluorine-containing copolymers broadly face notorious drawbacks of low fluorine content, poor fiber morphology and non-uniformity, hampering their application in sensor devices [118, 119]. For this reason, Mao et al. [111] originally proposed a thin porous microfiber membrane of platinum porphyrin grafted poly(isobutyl methacrylate-co-dodecafluoromethacrylate) copolymer with high fluorine content and applied it to an optical oxygen sensor (Fig. 8d, e). Unlike many solid sensor membranes, porous sensor membranes can promote the permeation of oxygen molecules, and the large surface area of fluorine in the fiber can offer more sites for analyte interactions and signal transduction [120, 121]. Therefore, the sensitivity of the fabricated optical gas sensor with a fluorine-containing microfiber membrane was greatly enhanced to be 584% higher than that of the solid sensor membrane.

Electrospun liquid crystal fiber mats have also been established to be a promising medium for gas sensing [122, 123]. Liquid crystals can operate at room temperature and do not require any input of energy as they are powered only by thermal energy and provide a strong optical response. They

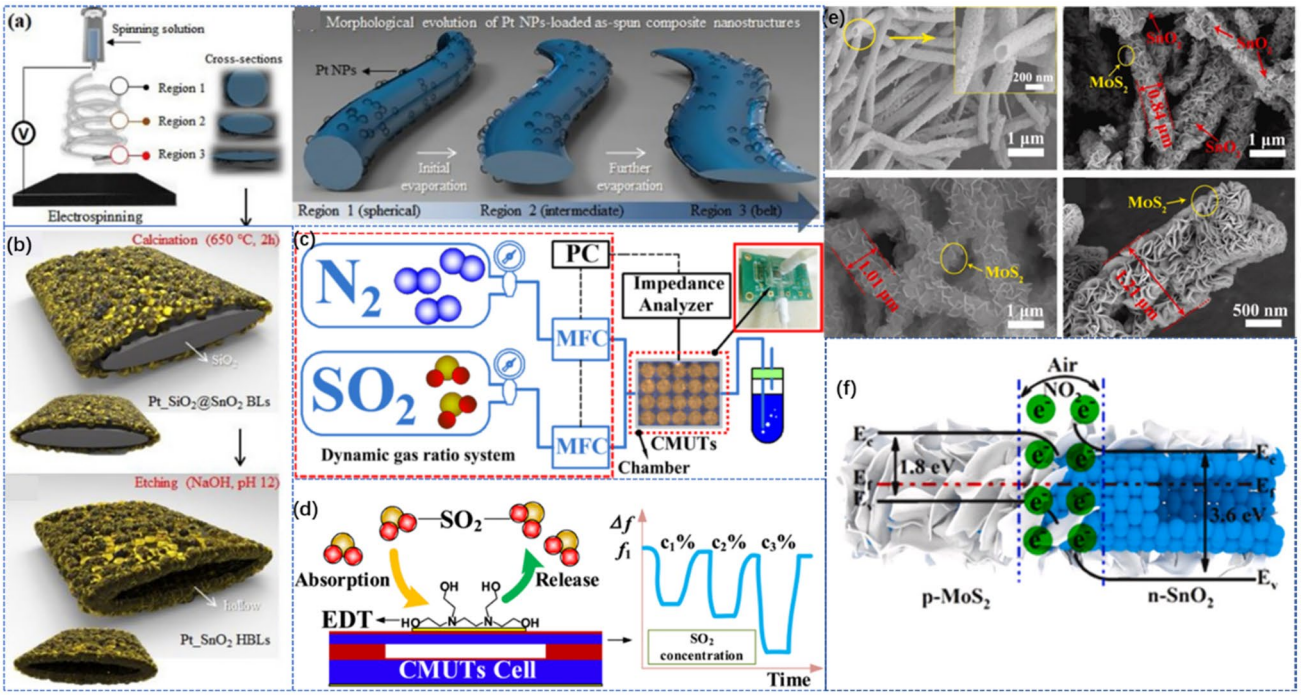

Fig. 6 Schematic illustrations of **a** morphological evolution about Pt NPs loaded as spun composite nanostructure and **b** morphology of Pt_SiO_2@SnO_2 belts obtained upon calcination and corresponding Pt_SnO_2 hollow belts obtained upon etching; reproduced with permission from ref. [96]; Copyright 2021, Elsevier. **c** Dynamic gas testing system and **d** the sensing mechanism of a CMUT-based resonant biochemical sensor; reproduced with permission from ref. [97], Copyright 2019, IEEE Industrial Electronics Society. **e** SEM images of pure SnO_2, MoS_2@SnO_2-1, MoS_2@SnO_2-2, and MoS_2@SnO_2-3 and **f** energy band structure of a nanocomposite of SnO_2 and MoS_2 in air and in NO_2 atmosphere; reproduced with permission from ref. [98], Copyright 2021, Elsevier

can conveniently detect gases without intricate spectroscopy equipment. Even low-concentration gases will strongly affect the self-assembly of liquid crystals [124, 125]. Reyes et al. [126] demonstrated the application of a polyvinylpyrrolidone-5CB fiber mat to qualitatively detect the presence of toluene gas by optical measurement. Wang et al. [127] suggested that the electrospun fiber mat made from polylactic acid (PLA) and amyl-cyanobiphenyl (5CB) could quantitatively detect toluene and acetone vapor. Agra-Kooijman et al. [128] reported a resistive liquid crystal core polymer fiber mat (LCC PFM) sensor, in which LC/polymer fibers were obtained after electrospinning on the IDE substrate. The results showed that they responded well to low concentrations of acetone at room temperature. These studies have revealed that chemicals can pass through the polymeric shell of the fiber and be absorbed by the liquid crystal in the core. Upon absorption, the optical properties of the fiber mat were altered by phase transition, which could be adopted for the sensitive and selective detection of volatile organic compounds.

Lead(II) acetate (($Pb(Ac)_2$) reacts with hydrogen sulfide to form a brown lead sulfide precipitate. Up to now, $Pb(Ac)_2$ has been used as an indicator in the form of test papers with a detection limit of 5 ppm to detect H_2S gas leaks. The Cha research group [129] successfully fabricated porous nanofibers with high surface area and thermal stability using $Pb(Ac)_2$, overcoming the limitations of traditional $Pb(Ac)_2$-based fibers H_2S sensors (Fig. 9). The nanostructure could not only prevent the aggregation of particles but also provided a variety of reaction sites. This sensor material detected H_2S as low as 400 ppb at 90% relative humidity.

QCM Gas Sensor

Quartz crystal microbalances (QCM) have attracted attention in gas detection owing to their high accuracy, low power consumption, and high stability. The detection mechanism is based on the load mass changes after the sensor layer absorbs gas molecules, which translates to changes in the resonant frequency of the quartz crystal [130–132]. The gas detection capability is highly dependent on the appropriate choice of nanomaterials, including metal oxides, organic polymers, and carbonaceous materials that make up the QCM sensor layer. For instance, a tungsten oxide film can detect NO_2, while graphene oxide can detect formaldehyde (HCHO) [133–135]. Despite the plethora of nanomaterials to select from, they lack porous structure and sufficient adsorption sites to absorb a considerable amount of target

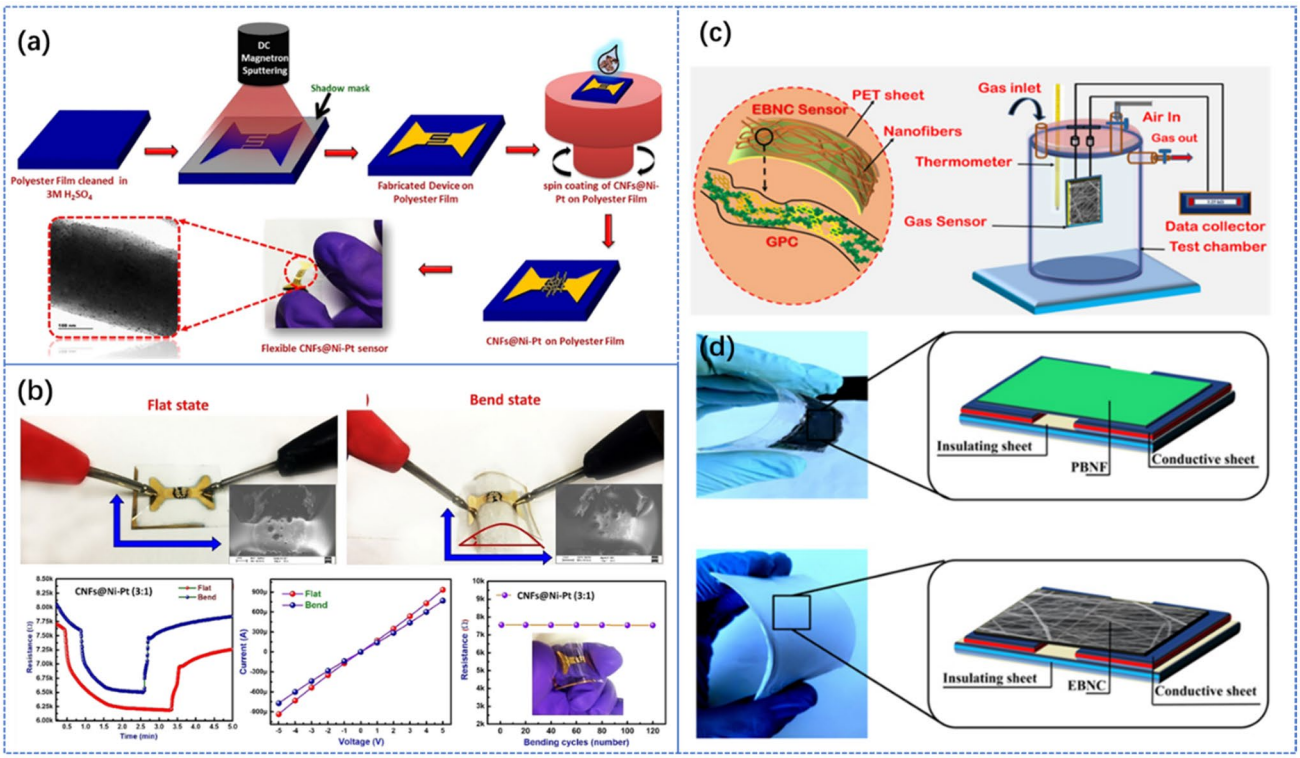

Fig. 7 **a** Fabrication process adopted for a CNF@Ni-Pt-based flexible hydrogen sensor and **b** photograph of the flexible CNFs@Ni-Pt (3:1)-based sensor; reproduced with permission from ref. [102], Copyright 2021, American Chemical Society. **c** Schematic of a homemade gas-sensing set-up used for evaluating gas sensors and **d** two gas sensors: one nanocomposite films based and the other EBNC based; reproduced with permission from ref. [103], Copyright 2021, IOP Publishing Ltd.

gas molecules. To further improve the ability of QCM sensor materials to absorb more gas molecules and their sensitivity, electrospinning technology has been introduced to produce highly porous sensor materials.

Kang et al. [136] used electrospinning and oxidative polymerization techniques to successfully prepare SnO_2 nanofibers (NFs)/PDA composites that were quantitatively deposited onto the QCM electrode surface. The SnO_2 nanofibers prepared in polymeric composites had rough morphology, which promoted the adsorption of gas molecules. The agglomerated PDA microspheres adhered to the surface of SnO_2 NFs and revealed a compact composite structure with a larger specific surface area exposing more active sites. The gas sensor prepared in this way showed a high sensitivity for formaldehyde sensing. Gas adsorption capacity is generally related to the surface functional groups and defect sites of the sensor materials. In addition to the porous nanofibers fabricated by electrospinning technology, the active metal oxides on the fiber surface were also crucial for gas adsorption, wherein the oxygen atom and imine functional group hydrogen-bonded with formaldehyde molecules [137, 138]. Moreover, the amine functional group in PDA nanospheres had undergone condensation with the aldehyde groups in formaldehyde to some extent [139, 140], thereby greatly improving the sensitivity. The fabricated nanofibrous QCM sensor achieved a detection limit of 500 ppb formaldehyde.

Diltemiz's research team [141] employed similar principles to prepare CuO-ZnO nanofibers for detecting formaldehyde as low as 41 ppb and the optimal detection frequency reached 8 Hz ppm^{-1}. Zhang et al. [142] made use of centrifugal electrospinning equipment to fabricate aligned nanofibers to selectively adsorb CO molecules against control nitrogen gas. Based on the Sauerbrey equation, it was found that an exceptionally high amount of CO (72.36 ng) was adsorbed on the nanofibers with a maximum frequency change of − 54 Hz for 50 ppm of CO feed, which was attributed to the large nanofiber surface area.

Metal Ion Sensor

Rapid industrialization is accompanied by several grim environmental problems, most notably water pollution [143]. Heavy metal pollution is a prevalent environmental issue that plays a detrimental role to aquatic life and human health [144, 145]. Therefore, society has paid close attention to the excessive discharge of heavy metal effluents because of their universality, trace-level toxicity, risk of carcinogenesis, and

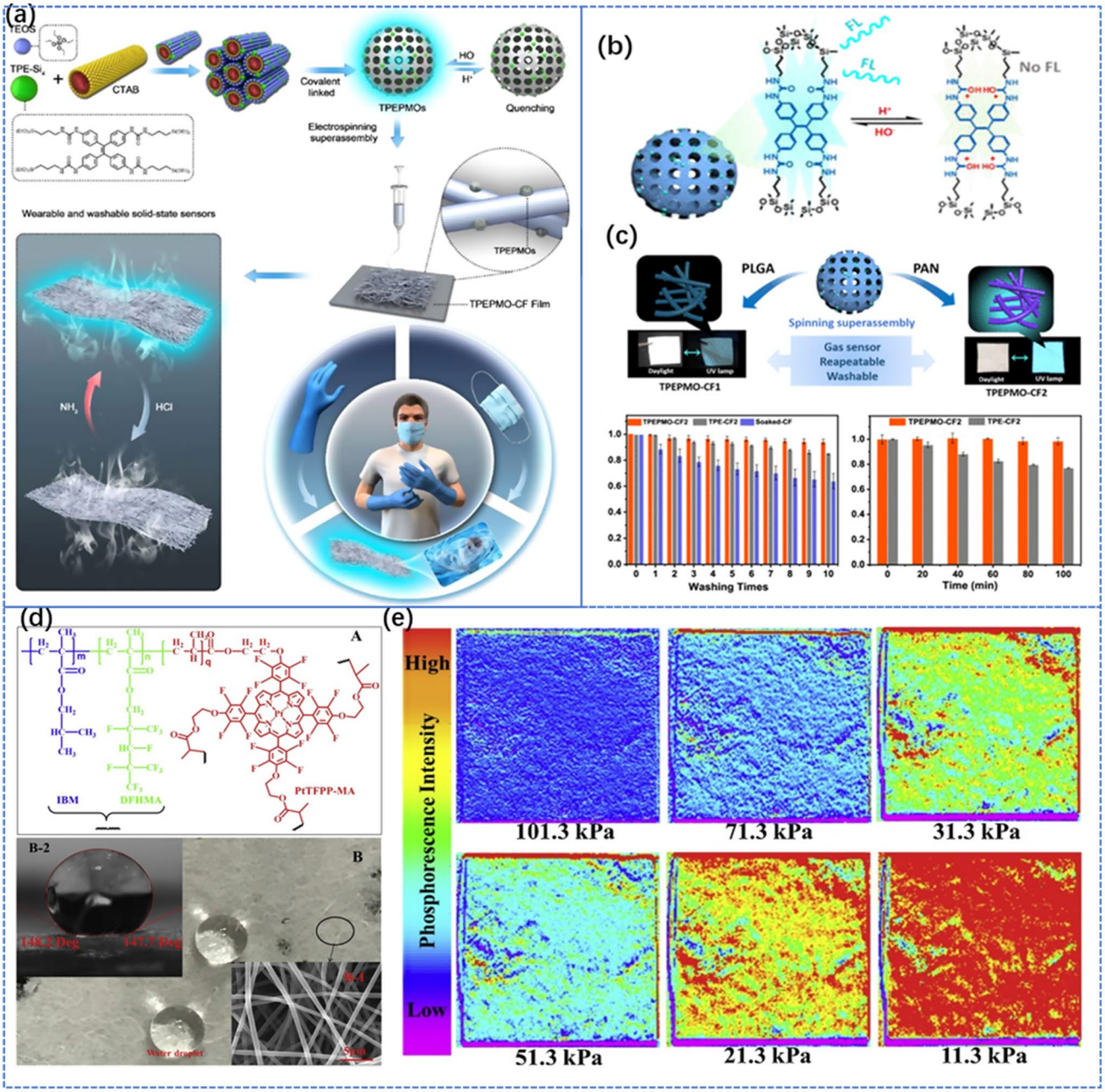

Fig. 8 **a** Schematic illustration of the construction of PMOs and PMO-CF films for sensor applications, **b** fluorescence sensing mechanism of PMOs and **c** optical properties of the PMO-CF film; reproduced with permission from ref. [110], Copyright 2021, American Chemical Society. **d** Chemical structure and photographs of contact angle measurement on the electrospun fibrous film and **e** the CCD images of microfiber films under photoluminescence excitation at different air pressures; reproduced with permission from ref. [111]; Copyright 2019, Elsevier

multiple organ failure. Table 1 lists the sources and effects of some highly toxic heavy metal ions that are the cause of many heavy metal-related diseases. In summary, in water pollution control, methods that can accurately monitor the heavy metals content in real time are of great significance for protecting the environment and human health [146].

Electrochemical Sensors

Electrochemical techniques have been extensively studied for their application in the detection and speciation of heavy metals. These electrochemical analyses normally use cyclic voltammetry (CV), differential pulse voltammetry (DPV), electrochemical impedance spectroscopy (EIS),

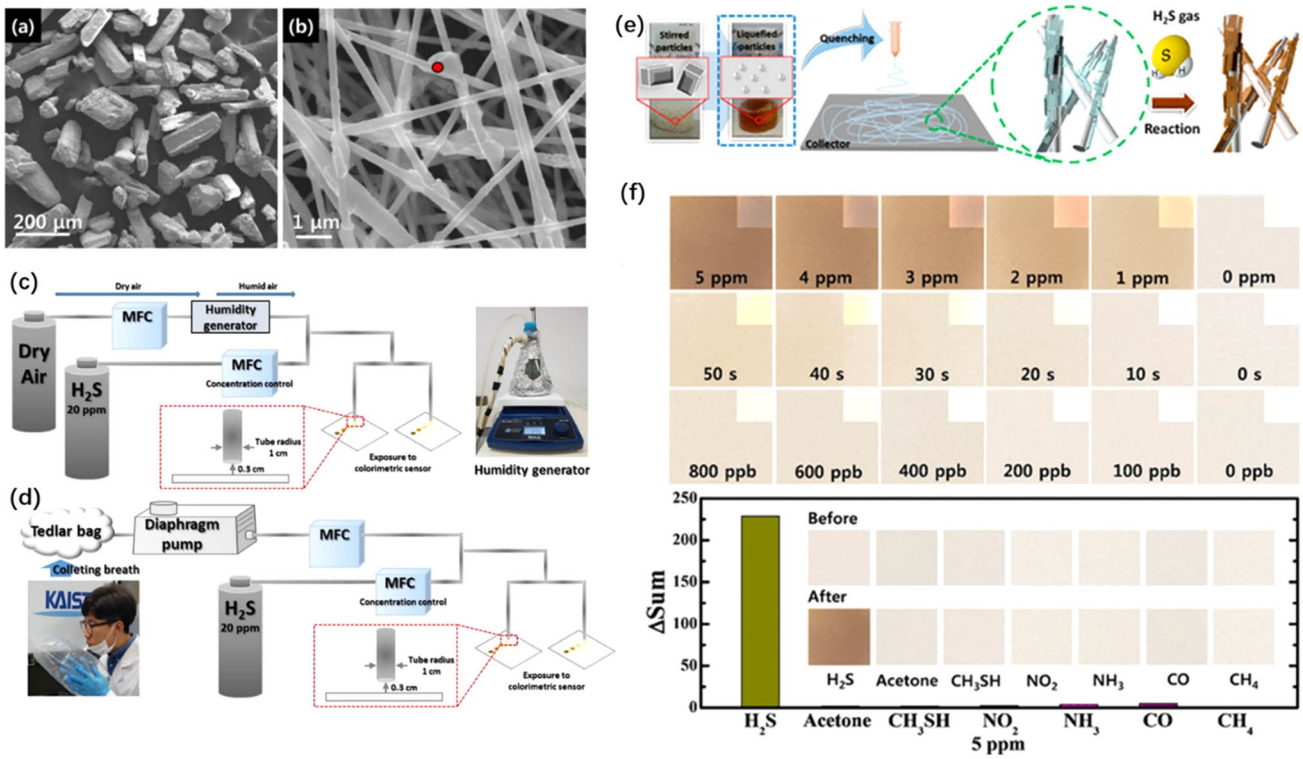

Fig. 9 SEM micrographs of **a** $Pb(Ac)_2$ particles and **b** $Pb(Ac)_2$@NFs; schematic representation of **c** the gas-sensing test and **d** simulated halitosis breath test equipment; **e** schematic illustrations of $Pb(Ac)_2$@NFs; **f** images of $Pb(Ac)_2$@NFs after exposure to various H_2S concentrations; reproduced with permission [129]; Copyright 2018, American Chemical Society

chronoamperometry (i–t), linear sweep voltammetry (LSV), and stripping voltammetry (SWSV) for that purpose. The measurements from the electrochemical analysis are typically registered as electrical signals such as resistance and current. Therefore, the electrochemical analysis equipment is relatively simple to analyze, easy to automate, and performs continuous analysis.

Chemically modified electrodes refer to the molecular design and modification of the electrode surface by chemical means to produce the electrode with specific electrochemical properties [159]. By endowing materials with excellent properties (catalytic effect, photoelectric effect, etc.) on the electrode surface, the conductivity of the electrode can be greatly improved, accelerating the electron transfer efficiency, while increasing the electrode response, thereby improving their selectivity and sensitivity as potential sensors [159, 160].

Common materials used in electrospinning are conductive polymers, carbonaceous, and metal nanoparticles [160]. Among the polymeric nanofibers, polyaniline (PANi) turned out to be the most commonly investigated conductive polymer owing to its one-dimensional structure that ensures high conductivity and surface area, which plays an extremely important role in the preparation of the electrode. Promphet et al. [161] uncovered the development of graphene/polyaniline/polystyrene (GO/PANi/PS) nanoporous fiber-modified screen-printed carbon electrode (SPCE), which was successfully solved by square wave anodic stripping voltammetry (SWASV) for the simultaneous determination of lead (Pb^{2+}) and cadmium (Cd^{2+}) in the range between 10 and 500 μg L^{-1}, with detection limits of 3.30 μg L^{-1} (Pb^{2+}) and 4.43 μg L^{-1} (Cd^{2+}). Similarly, Huang et al. [162] used phytic acid-doped polyaniline nanofiber-based nanocomposites to modify glassy carbon electrodes for Cd^{2+} and Pb^{2+} detection with EIS and differential pulse anodic stripping voltammetry (DPASV) proved that the synergistic effect of polyaniline nanofibers and phytic acid had enhanced the charge transfer efficiency of metal ions. Due to the synergistic effect of PANi, the detection limit of Cd^{2+} in the range of 0.0560 μg L^{-1} (S/N = 3) was 0.02 μg L^{-1}, and that of Pb^{2+} in the range of 0.160 μg L^{-1} was 0.05 μg L^{-1}.

Besides PANi, carbon nanofibers (CNFs) have attracted attention because of their high mechanical strength, large specific surface area, excellent electrical conductivity, and strong corrosion resistance. The PAN-based CNFs prepared by Zhao et al. [163] using electrospinning technology was eight times more sensitive to trace amounts of Pb^{2+} with a detection limit of 0.9 nM under anodic dissolution voltammetry analysis. Furthermore, Gao et al. [164] prepared nitrogen- and sulfur-codoped PAN-based CNFs by the pyrolysis

Table 1 The sources and side effects of some highly toxic heavy metal and emission limit values for heavy metal ions under the Chinese, WHO, and BIS regulations

Heavy metal	Source	Side effects	Emission limit (mg L^{-1})		
			GB 5749-2005[a]	WHO[b]	BIS[c]
Arsenic (As) [147, 148]	Mining, metallurgy, decolorizing agent, pesticide, chemical fertilizer, etc	Highly toxic Carcinogenicity	0.01	0.05	0.05
Cadmium (Cd) [149, 150]	Electroplating, mining, smelting, fuel, battery	Hypertension Cardiovascular and cerebrovascular disease Kidney failure	0.005	0.005	0.01
Chromium (hexavalent) (Cr(VI)) [151, 152]	Cosmetic raw materials, leather preparation, electroplating, industrial pigments, rubber	Cancer Liver damage Stomach ulcer Muscle spasm	0.05	0.05	0.05
Lead (Pb) [153]	Paint, coating, battery, smelting, electroplating, cosmetics, etc	Highly toxic Nervous System damage Intellectual damage	0.01	0.05	0.05
Mercury (Hg) [154, 155]	Instrument factory, salt electrolysis, smelting, cosmetics, dental materials, etc	Liver damage Nervous system damage Vision damage	0.001	0.001	0.001
Copper (Cu) [156, 157]	Smelting, metal processing, machinery manufacturing, rubber, etc	Gastrointestinal mucosa ulcer Hemolysis Liver necrosis Kidney damage	1	1.3	1.3
Zinc (Zn) [158]	Zinc mining, smelting, electroplating, machinery manufacturing, paper industry, etc	Diarrhea Nausea Vomiting	1	5	5

[a]Standards for drinking water quality (GB 5749-2005): Legal health standards for chemicals related to human health in drinking water issued by the Ministry of Health of China

[b]WHO: World Health Organization recommended permissible limits for heavy metal ions in water

[c]BIS: Permissible limits for heavy metal ions as per Bureau of Indian Standards

of trithiocyanuric acid and silica nanospheres, which showed the advantages of exhibiting large surface area (109 $m^2 g^{-1}$), porous structure and high proportion of heteroatoms (19 at.% of N and 0.75 at.% S). The electrochemical sensor fabricated using the high-performance porous CNFs was highly responsive to trace Cd^{2+} in the range of 2.0500 μg L^{-1} using DPASV. Tang et al. [165] formed PANi nanosheet arrays on electrospun Fe-CNFs substrates and deposited AuNPs uniformly on the nanosheet surfaces with reducing characteristics, which was shown in Fig. 10a, b. The presence of Fe in CNF accelerated the growth of PANi nanosheets and improved their adsorption of As^{3+}, responding to a wide linear range (5–400 ppb) and low detection limit of 0.5 ppb (S/N ≥ 3).

Metal oxides and metal nanoparticles are also widely applied in electrochemical sensors due to their significant electron transfer kinetic ability, larger specific surface area, and availability of adsorption sites [166]. ZnO is an excellent sensor material due to its high adsorption capacity, biocompatibility, and high chemical stability. The one-dimensional nanostructure can facilitate the diffusion of ions from the electrolyte to the surface of the sensor material more rapidly. Therefore, the production of nanofibers with highly uniform one-dimensional nanostructures by electrospinning is a feasible approach. Oliveira et al. [167] reported the synthesis of ZnO nanofibers/L-cysteine (ZnO/L-cys) nanocomposite electrode for electrochemical sensing of Pb^{2+}. Under the SWASV analysis, highly sensitive quantification of Pb^{2+} (LOD = 0.397 μg L^{-1}) was achieved in the linear range of 10,140 μg L^{-1}. Girija et al. [168] corroborated that cobalt and zinc ions form a stable tetrahedral structure with the zeolite imidazole ester framework under electrostatic action. On that basis, the cobalt–zinc–zeolite imidazole framework (Co/Zn-ZIF) nanofibers were successfully synthesized to detect heavy metal ions using CV analysis, uncovering the catalysis effect of the electrode to facilitate electron transfer between the electrode surface and metal ion. The Co/Zn-ZIF nanofibers effectively detected Cd^{2+} with low interference in the range from 100 nM to 1 mM and a detection limit of 27.27 nM. Teodoro et al. [169] used polyamide (PA6), cellulose nanowhiskers (CNW), and silver nanoparticles (AgNPs) to fabricate electrospun nanofiber electronic tongues for the quality assessment of water samples. It was found that the nanofiber mat was rich with pores and channels, which

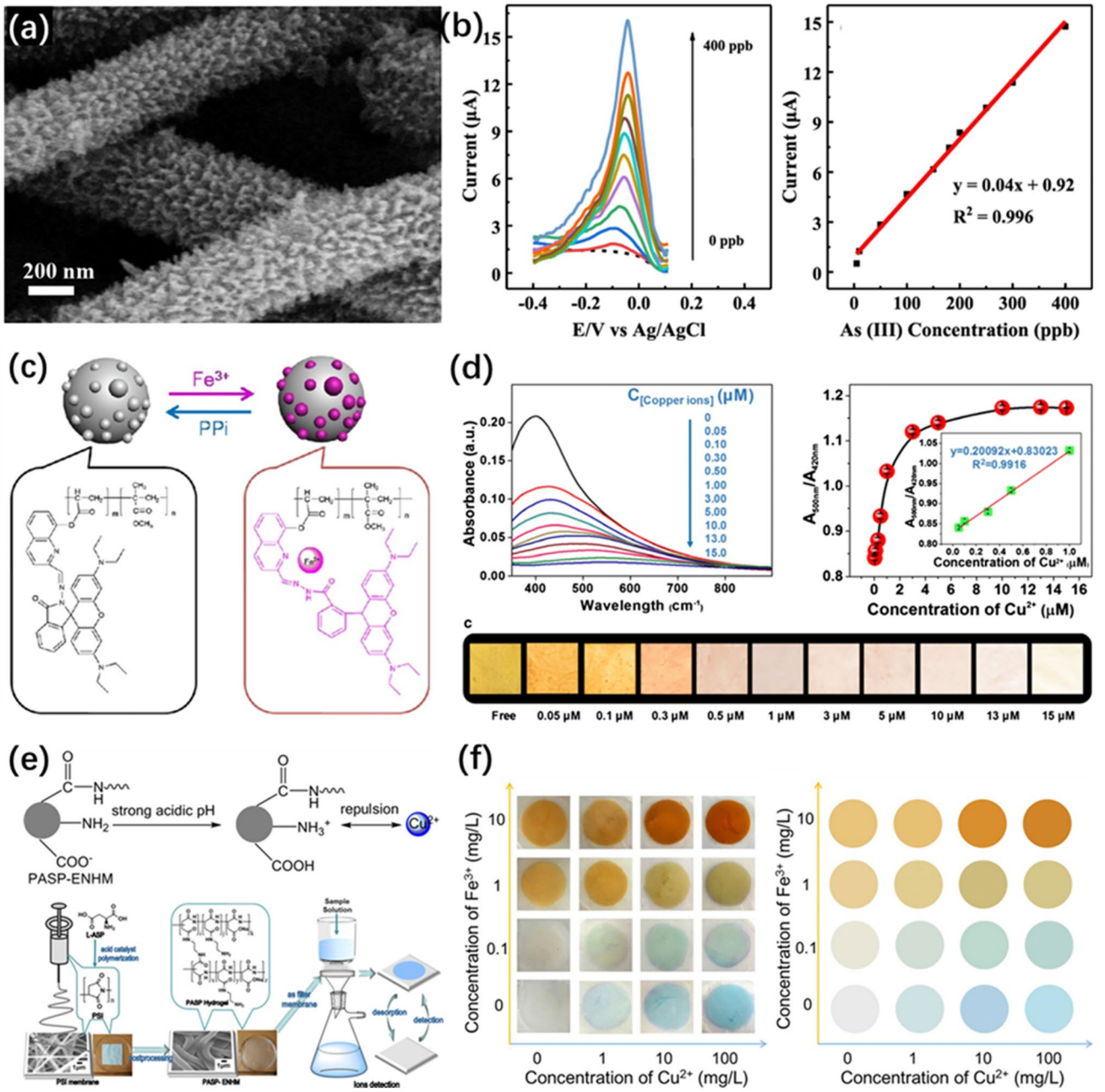

Fig. 10 **a** The morphology of Au–PANi–Fe–CNF and **b** the current response of As(III) in different concentrations; reproduced with permission from ref. [165], Copyright 2020, Elsevier. **c** The mechanism of colorimetric membrane; reproduced with permission from ref. [170], Copyright 2016, Elsevier. **d** Optical images of the sensor immersed in Au/Ag NPs colloid solution at different period; reproduced with permission from ref. [171], Copyright 2018, Springer Vienna. **e** Ion detection mechanism and **f** color-differentiation map about Fe^{3+} and Cu^{2+}; reproduced with permission from ref. [172], Copyright 2019, American Chemical Society

provided a multidisciplinary interaction between the binding site and analytes. With high aspect ratio, high biodegradability, and low density, CNW was uniformly blended in a co-system with metal nanoparticles for increased conductivity, enabling the prepared electronic tongue sensor to effectively discriminate different heavy metal ions with detection limit for Pb^{2+} in aqueous solution only 10 nM.

Colorimetric and Fluorescence Sensor

The binding constant of the analyte of interest and the nature of sensor molecules are the main factors affecting the sensitivity, specificity, reusability, and stability of the sensor. For the colorimetric sensor interface, the signaling molecule would need to induce responsive color change [173, 174].

Electrospinning has the advantages of fabricating a three-dimensional structure with a large specific surface area and excellent biocompatibility, which can provide more binding sites in the sensor molecules, and effectively improve the sensitivity and response rate of the sensor [174, 175]. Moreover, the low cost, simple operation and facile surface functionalization of electrospinning make it widely employed in many fields [176]. In recent years, colorimetric sensors constructed using electrospinning as the sensor interface have been used to detect metal ions with careful design of organic chemistry. Thence, with the development of nanotechnology, colorimetric methods based on surface plasmon resonance (SPR) of metal nanomaterials have progressively been introduced.

The core of the color sensing system is represented by the specific recognition molecules that can generate and transmit color signals, mainly using organic dyes or transition metal complexes. The recognition molecule and the analyte selectively interact by non-covalent bonding or covalent bonding, which induces the charge transfer or spatial structural change of the recognition molecule leading to the macroscopic manifestation in color change.

Rhodamine B (RhB), widely used for industrial coloring and as a fluorescent probe, is revealed to be a reliable color signal transmitter because of its long absorption and emission wavelengths, high photostability, high absorption coefficient, and quantum efficiency. Parsaee et al. [177] prepared Au NPs using *Gracilaria* under ultrasonication, and used electrospinning technology to modify silica gel membranes in the presence of RhB. The nanofibers immobilized with gold nanoparticles and RhB were used to detect Hg^{2+} in real water samples using colorimetry and fluorescence at detection limits of 2.21 nM and 1.10 nM, respectively. Moreover, the sensor can be reused multiple times with high integrity upon regeneration under oxidation by air. Similarly, Li et al. [170] used copolymers of rhodamine and quinoline propylene-based monomers to produce electrospun NFMs that acted as solid-state sensors and exhibited a high degree of Fe^{3+} selectivity, which was shown in Fig. 10c. In addition, the NFM realized the obvious color change from colorless to pink within a minute and its LOD was 1.19 μM.

Poly(aspartic acid) (PASP) is a synthetic poly(amino acid) with several unique properties, including strong metal ion binding ability, biocompatibility, biodegradability, water solubility, and low toxicity. Zhang et al. [172] developed a reuseable PASP-based colorimetric sensor with nanofiber structure for Cu^{2+} and Fe^{3+} detection, with a large amount of Cu^{2+} or Fe^{3+} accumulating on the PASP-based NFM after filtration, which was shown in Fig. 10e, f. Upon exposure to an aqueous Cu^{2+} solution, the color of the sensor changed from white to blue and the detection limit was reported to be 0.3 mg L^{-1}. In contrast, the membrane changed color from white to yellow, with a detection limit of 0.1 mg L^{-1} for Fe^{3+} aqueous solution.

Noble metal nanoparticles have a small size effect, surface effect, and quantum tunneling effect, and exhibit unique physicochemical properties. SPR can be described by the reaction of a large number of freely conducting electrons in precious metals to external incident electromagnetic waves. When the electronic oscillation frequency is equal to the incident light frequency, surface plasmon oscillation occurs, enabling the noble metal nanoparticles to produce strong absorption and scattering spectra in the visible light range. The spectral peak position is highly dependent on the size and distribution of the nanoparticles, and any changes in the external environment. When the radius of the nanoparticles is larger than 3.5 nm, the clustering of nanoparticles causes surface plasmon coupling, and a strong color change is observed in the visible light range.

The Au/Ag NPs were fixed on the aminated PAN nanofiber membrans (NFMs) to obtain a test strip with a porous structure of a large surface area (38.6 m^2 g^{-1}). The color of the NFM measured at a wavelength of 420 nm, underwent a redshift when exposed to Cu^{2+} and the color changed from yellow to pink to colorless. This effect was due to the leaching of Au/Ag NPs from NFM in the presence of ammonium chloride, thiosulfate, and Cu^{2+} and the formation of soluble thiosulfate complexes of Ag^{+}, Au^{3+}, and Cu^{2+}. On that basis, Abedalwafa et al. [171] achieved colorimetric detection of Cu^{2+} in drinking water samples by developing electrospun nanofiber membranes with Au/Ag core-shell nanoparticles, which was shown in Fig. 10d. Under optimized conditions, this method has the advantages of low detection limit (50 nM at S/N = 3), fast determination time (3 min), good specificity, and excellent reversibility.

Spectrometric Sensor

Surface-enhanced Raman Scattering (SERS) technology overcomes the inherent shortcomings of traditional Raman spectroscopy with weak signals and can increase the Raman intensity by several orders of magnitude. One of the main research directions in the SERS research area is the development of SERS substrates. The fabrication of SERS substrates usually relies on the surface plasmonic properties of the noble metal nanoparticles [178]. The nanoparticles loaded onto the electrospun polymer fiber mat, provides a larger surface area that can effectively enhance the detection signal and is considered to be an effective SERS substrate [179]. Xu et al. [180] fabricated a 3D SERS substrate composed of electrospun polycaprolactone (PCL) fibers and silver-coated gold nanorods (Ag/AuNRs) to detect traces of heavy metals in the environment. The successful fabrication and fixation of Ag/AuNRs on PCL fibers benefited from electrostatic interaction and excellent charge transfer between the gold

core and the silver layer in the bimetallic structure. Following that, the detection of trace concentrations of organic arsenic, arsenic acid and roxarsone was achieved. Zhang et al. [181] used electrospinning technology to produce for the first time polyacrylonitrile (PAN)/noble metal/SiO_2 nanofiber mats with plasma-enhanced fluorescence activity. These nanofiber mats selectively increased the fluorescence intensity of conjugated polyelectrolytes (CPE), making the polymer/noble metal nanofibers a promising substrate with improved sensitivity for metal ion detection.

Antibiotic Sensor

Since penicillin was discovered by Fleming in 1929 and used clinically by Florey and Chain, more than a hundred types of antibiotics have been developed and played a huge role in treating infectious diseases [182]. Antibiotics have an inhibitory effect on bacteria. Therefore, they are widely used to treat or prevent diseases in humans and animals [183]. Moreover, antibiotics are often added to animal feeds to promote animal growth and harvest. The types and properties of common antibiotics are listed in Table 2. Unfortunately, the problem of antibiotic contamination has become increasingly serious due to their mass production and abuse [184–186].

Antibiotics can enter the water environment in many ways and most commonly through urinary or fecal excretion [187]. The antibiotics discharged from the human body typically flow through the sewers and end up in the sewage treatment plant [186, 188]. However, the current sewage waste treatment technology could not completely remove antibiotics, causing residual antibiotics to be discharged from the sewage treatment plant and causing pollution of the aquatic environment and sources of drinking water [189–191]. Similarly, veterinary antibiotics cannot be completely metabolized and degraded in animals, and can enter the soil in the form of organic fertilizers and migrate to the ground- and surface water through runoff, infiltration, and leaching [192]. In this regard, antibiotics released into water bodies can affect the composition and activity of microorganisms, and detrimentally alter their ecological structure [193]. To make things worse, the challenge of bacterial resistance has been looming [191, 194], and the mixed consumption of antibiotics

Table 2 Types and properties of common antibiotics

Types of antibiotics		Chemical formula	Applications	Side effects
Tetracyclines [200, 201]	Tetracycline	$C_{22}H_{24}N_2O_8$	Mycoplasma	Gastrointestinal discomfort Liver toxicity
	Oxytetracycline	$C_{22}H_{24}O_9N_2$	Chlamydia infection	
	Doxycycline	$C_{22}H_{24}N_2O_8$	Lyme disease	
Aminoglycosides [202]	Gentamicin	$C_{60}H_{123}N_{15}O_{21}$	Gram-negative bacterial infections, such as *Escherichia coli*, Klebsiella, *Pseudomonas aeruginosa*	Hearing Damage Dizziness Nephrotoxicity
	Kanamycin	$C_{18}H_{36}N_4O_{11}$		
	Streptomycin	$C_{21}H_{39}N_7O_{12}$		
	Tobramycin	$C_{18}H_{37}N_5O_9$		
Macrolides [203]	Erythromycin	$C_{37}H_{67}NO_{13}$	Treatment of streptococcal infections, syphilis, respiratory tract infections, and mycoplasma infections	Nausea Vomiting Diarrhea
	Clarithromycin	$C_{38}H_{69}NO_{13}$		
	Dirithromycin	$C_{42}H_{78}N_2O_{14}$		
	Roxithromycin	$C_{41}H_{76}N_2O_{15}$		
	Azithromycin	$C_{38}H_{72}N_2O_{12}$		
β-Lactam [204, 205]	Pannixilin	$C_{16}H_{19}N_3O_5S$	Broad-spectrum antibacterial, streptococcal infection, syphilis	Gastrointestinal upset Diarrhea Severe allergies Kidney toxicity
	Ampicillin	$C_{16}H_{19}N_3O_4S$		
	penicillin	$C_{16}H_{18}N_2O_4S$		
	Azlocillin	$C_{20}H_{23}N_5O_6S$		
Quinolones [206, 207]	Ciprofloxacin	$C_{17}H_{18}FN_3O_3$	Urinary tract infections, bacterial prostatitis, bacterial diarrhea, gonorrhea	Nausea Tendon degeneration
	Levofloxacin	$C_{18}H_{20}FN_3O_4$		
	Norfloxacin	$C_{16}H_{18}FN_3O_3$		
	Ofloxacin	$C_{18}H_{20}FN_3O_4$		
Sulfonamides [208]	Trimethoprim	$C_{14}H_{18}N_4O_3$	Urinary tract infection	Nausea Vomiting Diarrhea Allergic rash Urinary stones Kidney failure
	Sulfamethizole	$C_9H_{10}N_4O_2S_2$		
	Sulfamethoxazole	$C_{10}H_{11}N_3O_3S$		

can cause the same kind of bacteria to develop resistance to multiple antibiotics, thus creating "Superbugs".

The detection techniques of antibiotics in trade effluents conventionally include capillary electrophoresis, spectrophotometry, SPR, gas chromatography and liquid chromatography, hyphenated techniques, and immunoassays [195–199]. The accuracy of the detection from these methods is very credible, with outstanding sensitivity and stability, but they place high demands on the instrument user and where sample preparation and operation procedures are often complicated and take a long time [191]. Therefore, on-site and real-time monitoring of antibiotics in the aquatic environment requires easy-to-operate and faster detection methods without compromising on their detection performance.

At present, there is not much research on using electrospinning technology to detect antibiotics, and the detection methods involved are still mainly focused on electrochemical detection and optical detection. The electrochemical detection method mainly includes two forms of representation: voltammetry and impedance. Non-specific bare electrodes typically limit the performance of the electrodes, modification strategies must be introduced to improve their performance. On the one hand, modifying the electrode surface by physical or chemical means can improve the hydrophilicity of the electrode–solution interface and thereby increase the concentration of antibiotics in the sensing area [209, 210]. Functional materials such as nanomaterials, organic materials, enzymes, or antibodies are assembled on the electrode surface through modification methods such as self-assembly, coating, electrodeposition, and electropolymerization. As a result, the modified electrode displays a special surface effect, size effect, quantum tunneling effect, and catalytic activity, which can enhance the conductivity of the electrode, accelerate the electron transfer in the interface, and reduce the redox overpotential of antibiotics [211, 212]. The effective amalgamation of the two above-mentioned aspects promotes a synergistic effect and significantly improves the sensitivity of antibiotic detection [182].

The three-dimensional porous network of CNFs network with extensive ion transport channels and a large aspect ratio facilitates the electron transport rate and effectively adjusts the charge diffusion length [213]. The composite structure formed of CNFs and other functional materials can significantly improve the surface chemical properties and conductivity, thereby changing its electron-donating ability and further improving the selectivity and stability of the sensor [214, 215].

Rare earth metal orthovanadate, among reported electrocatalysts, has become the most important functional material because of its tunable bandgap, abundant oxygen vacancies, non-cytotoxicity, excellent stability, and electrical conductivity. Baby et al. [195] presented a samarium vanadate/carbon nanofiber (SmV/CNF) composite material for the quantification of sulfadiazine (SFZ) over a wide linear range of 0.009–445 µM. The synergistic effect created by the composite structure of SmV and CNF accelerated the charge transfer while creating more active sites for detection. The prepared sensor had proven significant electrocatalytic activity, a low detection limit of 0.0013 µM, and high sensitivity of 4.03 µA μM^{-1} cm^2. In addition, Thangavelu Kokulnathan et al. [214] used zirconia/carbon nanofibers (ZrO_2/CNF) to fabricate a modified glassy carbon electrode (GCE), which was successfully applied for selective detection of chloramphenicol (CPL). DPV was used to measure the CPL reduction, which translates to quantification over a linear range from 0.005 to 903.76 µM with LOD of 0.0018 µM. Scagion et al. [216] assembled a new type of nanomaterial based on electrospun PA6/PANi nanofibers on a gold interdigital microelectrode and used it as the electronic impedance tongue sensing device to selectively detect tetracycline at a concentration as low as 1 ppb.

Selective sensing has always been the focus and bottleneck in antibiotic sensor development since their chemical structures can be very similar [217]. Common antigen-antibodies have strong specific binding ability despite the complicated antibody synthesis steps and strict storage conditions that have always limited their application in antibiotic sensors [218]. Easily synthesized and functionalized aptamers have been recognized as viable alternative sensing probes with high chemical stability [219, 220]. Song et al. [196] prepared a novel electrochemical aptamer sensor based on iron-based MOF that detected tetracycline in the range from 0.1 to 10^5 nM. CNFs based on the metal–organic framework NH_2-MIL-101(Fe) could not only provide more active sites to support the aptamer, the presence of amino groups (–NH_2) also promoted electron transfer and proton coupling [221]. Furthermore, NH_2-MIL-101(Fe) strongly interacted with the functional groups of the negatively charged nucleic acid sequence, which allowed it to capture a considerable amount of target pollutants, thereby improving the sensitivity of the electrochemical sensor [222, 223]. Similarly, Vafaye et al. [224] electrodeposited gold nanoparticles on the surface of a carbon nanofiber mat to fix the aptamer, realizing a highly sensitive detection of penicillin (1–400 ng mL^{-1}).

Among the optical sensors, colorimetry is the most intuitive detection method and, Fe^{3+} is commonly utilized in this instance to drive color change. The chemical structure of tetracycline is highly prone to complex with the Fe atoms as it contains multiple O- and N-containing functional groups [225, 226]. The oxygen atoms of the carboxylate in the alginate skeleton preferentially chelate to Fe^{3+} that eventually bind to the target antibiotic molecules. Based on this principle, Yan et al. [227] functionalized alginate directly on the surface of PAN nanofibers for Fe^{3+} fixation and detected 5 µg kg^{-1} of tetracycline (TC) within 10 min with a color

change that could be observed easily with the naked eyes, which was shown in Fig. 11a, b.

Due to its highly effective antibacterial properties, metronidazole (MTZ) is widely used as a food additive in animal husbandry to promote the growth of animals and plants. However, MTZ can cause serious diseases through genotoxic, carcinogenic, and mutagenic effects [228]. Therefore, appropriate detection methods are required to prevent excessive MTZ residues from entering o the aquatic environment, which would adversely affect human health. Under neutral pH, the amino groups in melamine (MA) form a covalent bond with the Au nanoparticles with increased stability. When MTZ binds with the composite material (MA@GNP) via hydrogen bonding, the color of MA@GNP changes from pink to purple due to the aggregation of gold nanoparticles. Mohammed et al. [229] reproduced this phenomenon by assembling melamine-functionalized Au nanoparticles on polyamide NFMs. The resulting colorimetric strips, which shown in Fig. 11c, d showed good sensitivity for MTZ with low LOD (2 nM at S/N = 3) and a fast response time (2.5 min).

Apart from colorimetry, SERS is also a powerful spectroscopy technique that can be used for label-free detection of (bio)chemical substances. The principle behind this technology is the electromagnetic amplification by noble metal nanostructures as mentioned previously. Kang et al. [230] reported a SERS sensor based on assembled Au@Ag core-shell nanoparticles on an electrospun nanofiber matrix that was used for the selective detection of methamphetamine at logarithmic concentration from 10^{-1} to 10^{4} ppb, with the detection limit reaching an impressive 7.2 ppt. Tang et al. [231] further found that amorphous silica nanofibers uniformly loaded with Ag nanoparticles fabricated using electrospinning technology showed strong SERS enhancement effects and achieved high efficiency for trace antibiotics detection.

Pesticide Sensor

There have been reports of pesticide pollution of the aquatic environment around the world [232, 233]. According to reports, many famous rivers such as the Yangtze River, Songhua River, Tingjiang River, and Heilongjiang River in China have been polluted by pesticides. More than 130 pesticides or their degraded products have also been identified in groundwater in the United States. Pesticide residues such as atrazine, acetochlor, and dimehypo were found in groundwater in Jiangsu, Jiangxi, and Hebei, China. In

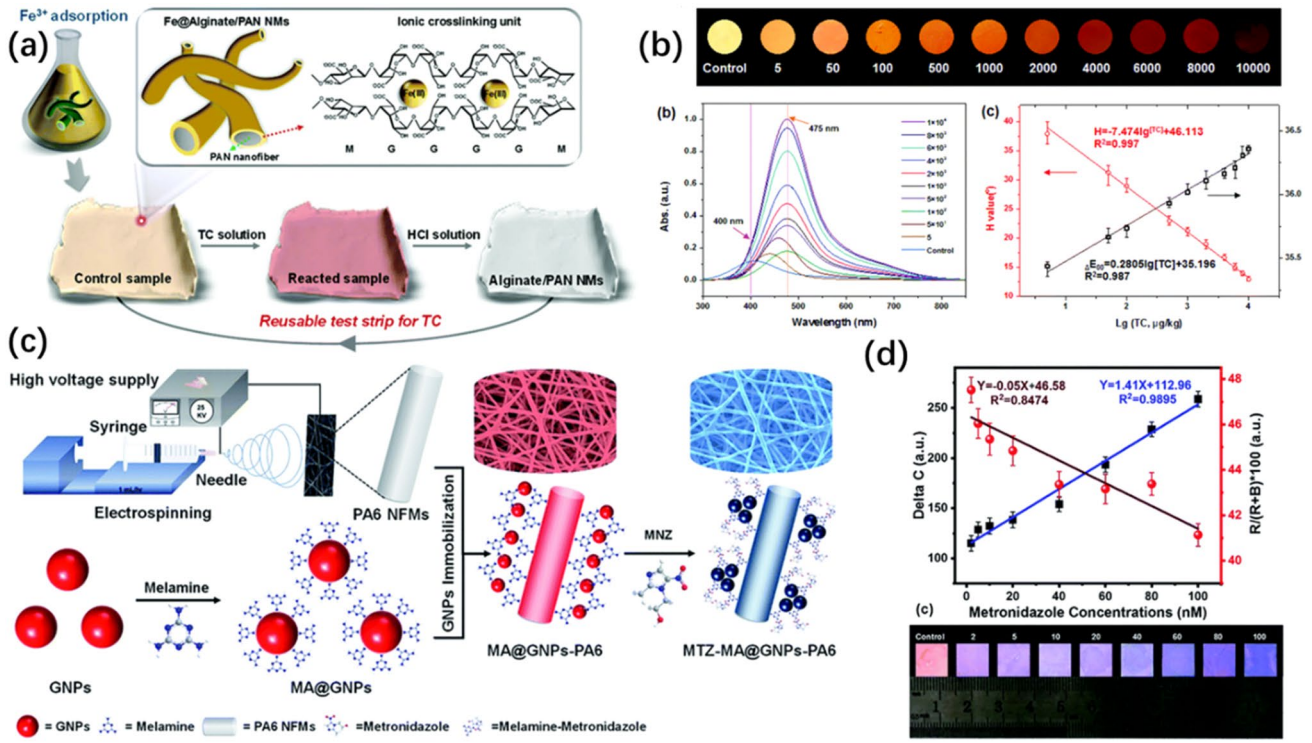

Fig. 11 **a** Three stages scheme of the colorimetric strips for TC determination, **b** the visual colorimetric response and the UV-Vis spectra of the strips against different concentrations of TC; reproduced with permission from ref. [227], Copyright 2018, Royal Society of Chemistry. **c** Illustration of the design, fabrication, and detection mechanism of the MA@GNP-immobilized PA6 NFM colorimetric strips for metronidazole and **d** the linear relationship between the color difference values; reproduced with permission from ref. [229], Copyright 2019, Royal Society of Chemistry

general, the higher the water solubility of pesticides, the more residues can be found in the water and studies have shown that surface waters can easily promote the accumulation of pesticides or chemical substances [234]. Additionally, the pollutants in the surface water are easily displaced to the groundwater through the hydrological cycle or soil infiltration. Therefore, pollution of the aquatic environment caused by pesticides is a very urgent global issue to be addressed.

Today, the detection of pesticides in the aquatic environment relies mainly on manual on-site sampling and then routine analytical techniques such as gas chromatography and high-performance liquid chromatography [235–237]. It is undeniable that chromatography is highly accurate and a mature detection technology, but the underlying factors such as expensive instrumentation, cumbersome sample preparation process, and high operational requirements make pesticide detection challenging. Over the past 5 years, a variety of rapid detection methods have been developed, including electrochemical sensors, colorimetric sensors, and detection cards [232, 238]. These new detection technologies help environmental inspectors to localize the pollutants in the aquatic environment in time, and effectively avoid the large-scale release and spread of pollutants.

Feng et al. [238] combined electrospinning and hydrophilic modification to develop an emerging type of nano-/microstructure detection card based on PCL fiber mats to detect indole acetate and acetylcholinesterase (AChE). Pretreating the fiber mat with ethanol promoted hydrolysis of the PCL fiber mat, which improved the surface wettability, and the minimum detectable concentrations of carbofuran, malathion, and trichlorfon were reduced by fivefold, twofold, and 1.5-fold, respectively (Fig. 12a, b). Using a similar approach, Moghazy et al. [239] electrospun chitosan/PVA nanofibers to fabricate a mutant acetylcholinesterase-based biosensor with LOD determined to be 0.2 nM for phosphorus and thus far below the maximum residue limit (MRL) of 164 nM, set by international regulations. The low LOD could be achieved owing to the unique spatial structure, high porosity, and large specific surface area of the electrospun fibers. Shao et al. [240] used electrospinning technology to manufacture flexible and hydrophobic Ag/SB nanofiber films as SERS substrates on a large scale. Using R6G as a probe molecule, it was observed that the Ag/SB-SERS method had excellent sensitivity and stable signal reproducibility towards triazophos with LOD of 2.5×10^{-8} M. More importantly, the method did not require complicated sample preparation.

Atrazine is a type 3A carcinogen and an insecticide in the chlorotriazine family, and is known to seriously affect the human endocrine system if consumed. The high toxicity of atrazine extends its effect on animals and plants. Supraja et al. [232] electrospun SnO nanofibers to perform label-free, and ultra-sensitive electrochemical detection of atrazine within the wide dynamic detection range of μM, achieving a detection limit for atrazine of 0.9 zM and sensitivity of 4.11 μA μM^{-1} cm^{-2} (Fig. 12c, d).

Nitrophenols, including three isomers *o*-nitrophenol (*o*-NP), *m*-nitrophenol (*m*-NP), and *p*-nitrophenol (*p*-NP), are all important raw materials for the production of pesticides and are suspected carcinogens [241]. They have high chemical stability and will not be easily degraded by microorganisms, which seriously upset the ecosystem balance [242], hence are listed by the United States Environmental Protection Agency (USEPA) as toxic pollutants and hazardous wastes of top priority. According to the European Communities Commission regulations, the maximum allowable amount of nitrophenol in drinking water is 5.0 μM [243–245]. Unfortunately, *o*-NP and *p*-NP as hydrolysates of pesticides (parathion and methyl parathion, etc.) widely contribute to water and food contamination and are commonly used as markers to diagnose pesticide contamination [246]. Zhu's research group [247] prepared CNFs with a high surface area–volume ratio and aspect ratio by the carbonization of electrospun PAN fibers. By controlling the polymerization time and ammonium persulfate (APS) feed rate, a one-dimensional nanoconical PANi array with favorable uniformity was successfully assembled on the electrospun CNFs (PANi-array@CNF) at low temperatures yielding abundant mesoporous structures necessary for electrochemical reactions (Fig. 12e–g). Due to the large specific surface area and highly ordered nanostructure, the CNF electrode displayed excellent activity and response to the electrochemical reduction of nitrophenol, enabling ultra-sensitive and selective detection of *p*-nitrophenol with a LOD as low as 1.5 nM. Moreover, the fabricated sensor could quantify and differentiate *o*-NP and *p*-NP simultaneously. Antohe et al. [248] reported a PANi/platinum coating for the highly sensitive detection of 4-nitrophenol (4-NP) contaminant with a layered fiber surface plasmon resonance sensor, which revealed excellent detection performance in the low picomolar range (LOD = 0.34 pM).

Others

The composition of pollutants in the aquatic environment is complex. Besides chemical pollutants, biological contamination such as bacteria, viruses, and parasites are of high prevalence and relevance today. Schistosomiasis is one of the deadliest diseases caused by parasites from water pollution and their transmission can be much faster than chemical contamination to cause an outbreak of diseases.

The Coronavirus Disease 2019 (COVID-19) pandemic has taken millions of lives worldwide and there is a need to rapidly detect the virus. Currently, real-time (quantitative) reverse transcription polymerase chain reaction (RT-PCR) is considered the gold standard for COVID-19 diagnosis.

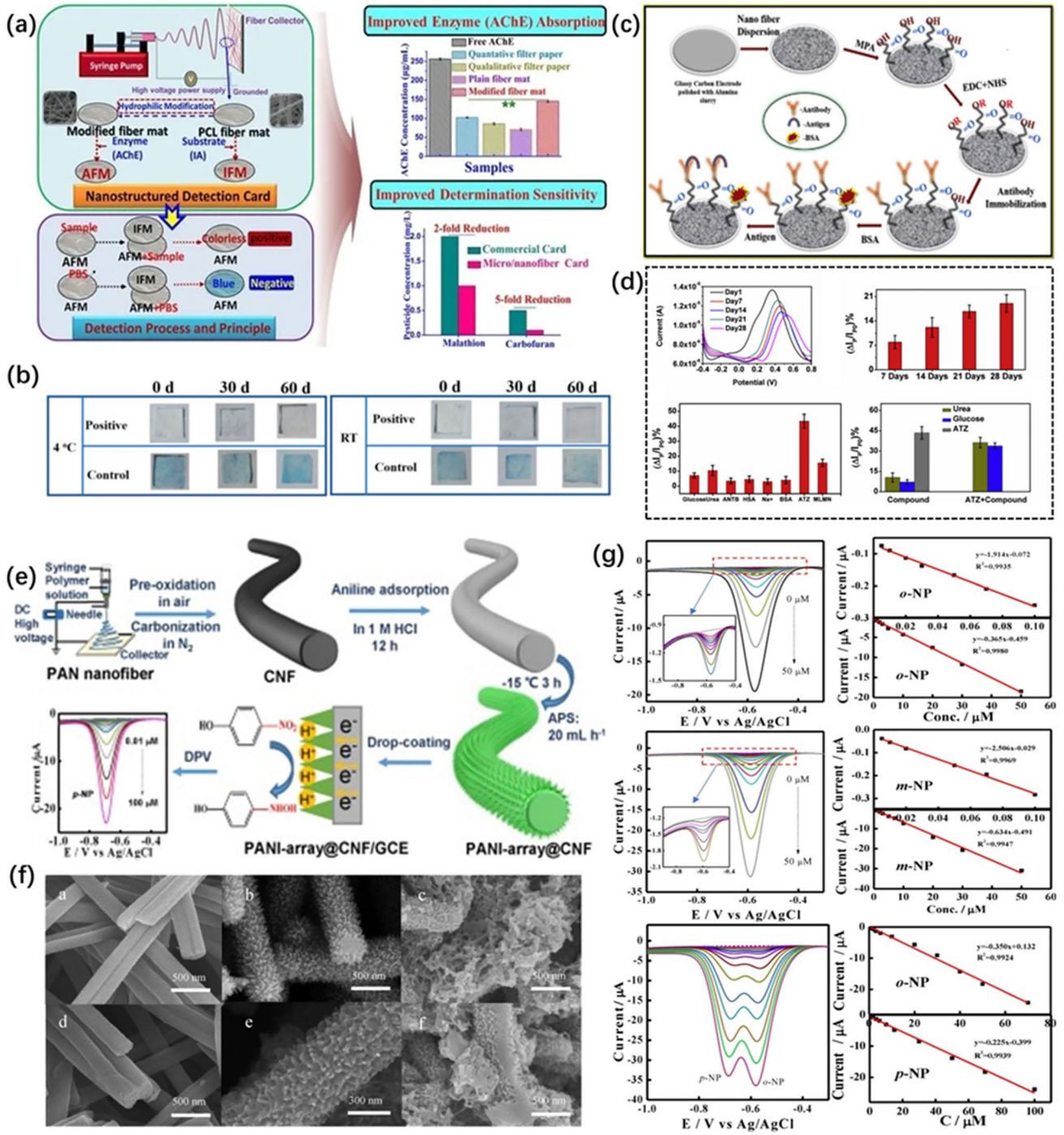

Fig. 12 **a** The preparation process and principle of pesticide determination of the nano-/microstructured detection card and **b** storage stability of the detection card below 4 °C and room temperature (RT); reproduced with permission from ref. [238], Copyright 2021, MDPI. **c** Schematic representation of the proposed biosensor platform and **d** the stability, selectivity, and interference suppression of the immobilized electrode; reproduced with permission from ref. [247], Copyright 2019, Elsevier. **e** Schematic illustration of the synthesis process of PANi-array@CNF, **f** FE-SEM micrographs of PANi-array@CNF prepared at different feeding speeds, and **g** DPVs of the PANi-array@CNF/GCE with different concentrations of *o*-NP, *m*-NP and simultaneous addition of different concentrations of *o*-NP and *p*-NP; reproduced with permission from ref. [232], Copyright 2020, Elsevier

However, RT-PCR-based tests are complex, expensive, time-consuming, and require sample pre-treatment by trained personnel. Over the past 2 years, researchers around the world have developed several solutions to quickly diagnose COVID-19. However, in the early stages of infection, there are many false-positive misdiagnoses with these developed sensors. To address the current challenges, Jadhav et al. [249] proposed a diagnostic scheme based on SERS combined with microfluidics integrating microchannels. The channels consisted of Au/Ag-coated carbon nanotubes and an electrospun micro/nanofiltration membrane reported to have the potential to successfully capture viruses from various biological fluids/secretions.

In other instances of monitoring biological contaminants, Xu et al. [250] reported a novel type of aptamer@AuNPs@UiO-66-NH_2 nanofiber sensor for specific detection of microcystin (MC-LR). High loading of MOFs and aptamers on nanofiber fibers was achieved and successfully applied to accurately identify MC-LR by solid-phase microextraction (SPME) combined with LC–MS. Highly specific recognition of MC-LR was achieved with an extremely low LOD (0.004 ng mL^{-1}) and good precision (CV% < 11.0%). Yang et al. [251] used the electrospun nanofiber mat prepared by the in situ assembly of tunable Ag nanoparticles on TiO_2 nanofibers to detect bacteria. The Ag NPs were uniformly deposited on the nanofibers on the surface of TiO_2 so that the composite nanofiber mat had excellent SERS properties. The minimum detection limit of the sensor was around 10^{-9} mol L^{-1}. More importantly, the nanofiber mat fabricated could be used as a SERS substrate to detect *E. coli*, *S. aureus* and other biological macromolecules without the need for using aptamers. Niri et al. [252] developed a CNF-based electrochemical biosensor for the detection of Hepatitis B virus in a linear range of 10^{-12}–10^{-6} M, with a detection limit of 1.58×10^{-12} M. Arshad et al. [253] developed an impedance sensor based on molecularly imprinted polymer (MIP) and electrospun PS nanofibers for early detection of dengue infection, successfully attaining a linear response ranging from 1 to 200 ng mL^{-1}, and the LOD as low as 0.3 ng mL^{-1}.

Conclusion and Future Trends

In the present comprehensive review, electrospinning technology has been uncovered to be one of the most effective methods that can be used to achieve mass production of nanofibers for different applications. Electrospun nanofiber membrane is empowered with the advantages of displaying three-dimensional structure, high porosity, large specific surface area, and controllable structure. It is an ideal nanomaterial for fabricating high-performance sensor elements. Compared to methods such as hydrothermal and templating, electrospinning allows the blending and in situ polymerization or cross-linking, of a variety of functional materials to realize the preparation of nanomaterials with unique structures and morphologies including nanofibers, nanowires (nanorods), nanoribbons, hollow nanofibers, core-shell structures, hollow nanotubes, and nanodendrites. Moreover, these electrospun nanomaterials have high axial strength and can facilitate continuous electron transfer along the long-axis direction, so that they can achieve higher sensitivity in the field of environmental sensing. Finally, the electrospinning technology is easy to mass-produce and commercialize, laying the foundation for the market application of nanofiber-based sensors in the near future.

Although the prospects are optimistic, there are many challenges ahead in bringing sensors based on electrospinning technology into the market and realizing industrial-scale production. These include: (1) improving the dispersion of nanomaterials on the surface or inside nanofibers so that the functionalized materials are evenly distributed; (2) the fabrication of electrospun nanofibers is highly susceptible to environmental factors, and the process of nanofibers needs to be improved. Parameters to ensure the stability and repeatability of nanofibers produced under large-scale manufacturing conditions; (3) the integration of electrospinning nanofibers with chips, wearable devices, and other sensor platforms; (4) at this stage, the laboratory-based environmental sensors are only used for detection in a relatively clean gas and water environment, and the actual environment contains much more complex interferences, which poses requirements for the selectivity and anti-interference of the sensor; and (5) environmental sensors are mainly divided into real-time detection and long-term monitoring. Long-term monitoring in particular poses a challenge to the stability of the sensor.

In conclusion, nanofibers produced by electrospinning technology offer many effective binding sites for analytes due to their high surface area and porosity, which greatly improves the sensitivity and response time of the sensor. Despite the evident challenges, the authors have great confidence that the future commercialization of electrospinning technology for environmental monitoring can be expected with the continuous research efforts.

Acknowledgements This work is supported by the National Key Research and Development Project (2019YFC0408304), the Fundamental Research Funds for the Central Universities and Graduate Student Innovation Fund of Donghua University (no. 2232022G-04, BCZD2022005, and CUSF-DH-D-2021037). The support provided by China Scholarship Council (CSC) (no. 202006630085) during a visit to the National University of Singapore is also acknowledged.

Declarations

Conflict of Interest On behalf of all authors, the corresponding author states that there is no conflict of interest.

References

1. Liang LW, Wang ZB, Li JX. The effect of urbanization on environmental pollution in rapidly developing urban agglomerations. *J Clean Prod* **2019**;*237*:117649.
2. Chowdhary P, Raj A, Bharagava RN. Environmental pollution and health hazards from distillery wastewater and treatment approaches to combat the environmental threats: a review. *Chemosphere* **2018**;*194*:229.
3. Manisalidis I, Stavropoulou E, Stavropoulos A, Bezirtzoglou E. Environmental and health impacts of air pollution: a review. *Frontiers Public Health* **2020**;*8*:14.
4. Novo A, Andre S, Viana P, Nunes OC, Manaia CM. Antibiotic resistance, antimicrobial residues and bacterial community composition in urban wastewater. *Water Res* **1875**;*2013*:47.
5. Cheng DL, Ngo HH, Guo WS, Chang SW, Nguyen DD, Liu YW, Wei Q, Wei D. A critical review on antibiotics and hormones in swine wastewater: water pollution problems and control approaches. *J Hazard Mater* **2020**;*387*:121682.
6. Cacace D, Fatta-Kassinos D, Manaia CM, Cytryn E, Kreuzinger N, Rizzo L, Karaolia P, Schwartz T, Alexander J, Merlin C, Garelick H, Schmitt H, de Vries D, Schwermer CU, Meric S, Ozkal CB, Pons MN, Kneis D, Berendonk TU. Antibiotic resistance genes in treated wastewater and in the receiving water bodies: a pan-European survey of urban settings. *Water Res* **2019**;*162*:320.
7. Sutka A, Gross KA. Spinel ferrite oxide semiconductor gas sensors. *Sens Actuators B Chem* **2016**;*222*:95.
8. Fang X, Zong BY, Mao S. Metal-organic framework-based sensors for environmental contaminant sensing. *Nano Micro Lett* **2018**;*10*:92–110.
9. Li M, Gou HL, Al-Ogaidi I, Wu NQ. Nanostructured sensors for detection of heavy metals: a review. *Acs Sustain Chem Eng* **2013**;*1*:713.
10. Qi YY, Chen YT, Xiu FR, Hou JX. An aptamer-based colorimetric sensing of acetamiprid in environmental samples: convenience, sensitivity and practicability. *Sens Actuators B Chem* **2020**;*304*:127359.1–127359.8.
11. Zhu L, Wang JN, Liu JW, Nasir MS, Zhu JW, Li SS, Liang JD, Yan W. Smart formaldehyde detection enabled by metal organic framework-derived doped electrospun hollow nanofibers. *Sens Actuators B Chem* **2021**;*326*:128819.
12. Ding JX, Zhang J, Li JN, Li D, Xiao CS, Xiao HH, Yang HH, Zhuang XL, Chen XS. Electrospun polymer biomaterials. *Prog Polym Sci* **2019**;*90*:1.
13. Wang XX, Yu GF, Zhang J, Yu M, Ramakrishna S, Long YZ. Conductive polymer ultrafine fibers via electrospinning: preparation, physical properties and applications. *Prog Mater Sci* **2021**;*115*:100704.
14. Chen SX, Li RQ, Li XR, Xie JW. Electrospinning: an enabling nanotechnology platform for drug delivery and regenerative medicine. *Adv Drug Deliv Rev* **2018**;*132*:188.
15. Ghosal K, Agatemor C, Spitalsky Z, Thomas S, Kny E. Electrospinning tissue engineering and wound dressing scaffolds from polymer-titanium dioxide nanocomposites. *Chem Eng J* **2019**;*358*:1262.
16. Liu Q, Zhu JH, Zhang LW, Qiu YJ. Recent advances in energy materials by electrospinning. *Renew Sustain Energy Rev* **1825**;*2018*:81.
17. Sun B, Long YZ, Zhang HD, Li MM, Duvail JL, Jiang XY, Yin HL. Advances in three-dimensional nanofibrous macrostructures via electrospinning. *Prog Polym Sci* **2014**;*39*:862.
18. Greiner A, Wendorff JH. Electrospinning: a fascinating method for the preparation of ultrathin fibres. *Angew Chem Int Ed* **2007**;*46*:5670.
19. Li D, Xia YN. Electrospinning of nanofibers: reinventing the wheel? *Adv Mater* **2004**;*16*:1151.
20. Xue JJ, Wu T, Dai YQ, Xia YN. Electrospinning and electrospun nanofibers: methods, materials, and applications. *Chem Rev* **2019**;*119*:5298.
21. Ahmed FE, Lalia BS, Hashaikeh R. A review on electrospinning for membrane fabrication: challenges and applications. *Desalination* **2015**;*356*:15.
22. Zhang H, Liu YN, Cui K, Zhao QL, Huang J, Mao SH, Jiang T, Ma Z. Electrospun ribbon-like microfiber films of a novel guanidine-based ABA triblock copolymer: fabrication, antibacterial activity, and cytotoxicity. *Macromol Chem Phys* **2019**;*220*:1900138.
23. Gangolphe L, Leon-Valdivieso CY, Nottelet B, Dejean S, Bethry A, Pinese C, Bossard F, Garric X. Electrospun microstructured PLA-based scaffolds featuring relevant anisotropic, mechanical and degradation characteristics for soft tissue engineering. *Mater Sci Eng C Mater Biol Appl* **2021**;*129*:112339.
24. Liang M, Hebraud A, Sutter C, Bardin A, Lobry E, Schlatter G. Measurement and modeling of the nanofiber surface potential during electrospinning on a patterned collector: toward directed 3D microstructuration. *Adv Mater Interfaces* **2021**;*8*:2101302.
25. Park SH, Kim MS, Lee B, Park JH, Lee HJ, Lee NK, Jeon NL, Suh KY. Creation of a hybrid scaffold with dual configuration of aligned and random electrospun fibers. *ACS Appl Mater Interfaces* **2016**;*8*:2826.
26. Shin MK, Kim SI, Kim SJ. Controlled assembly of polymer nanofibers: from helical springs to fully extended. *Appl Phys Lett* **2006**;*88*:223109.
27. Kongkhlang T, Kotaki M, Kousaka Y, Umemura T, Nakaya D, Chirachanchai S. Electrospun polyoxymethylene: spinning conditions and its consequent nanoporous nanofiber. *Macromolecules* **2008**;*41*:4746.
28. Park KR, Cho HB, Lee J, Song Y, Kim WB, Choa YH. Design of highly porous SnO_2–CuO nanotubes for enhancing H2S gas sensor performance. *Sens Actuators B Chem* **2020**;*302*:127179.
29. Lin MF, Xiong JQ, Wang JX, Parida K, Lee PS. Core-shell nanofiber mats for tactile pressure sensor and nanogenerator applications. *Nano Energy* **2018**;*44*:248.
30. Wang LG, Topham PD, Mykhaylyk OO, Yu H, Ryan AJ, Fairclough JPA, Bras W. Self-assembly-driven electrospinning: the transition from fibers to intact beaded morphologies. *Macromol Rapid Commun* **2015**;*36*:1437.
31. Zhang CL, Yu SH. Nanoparticles meet electrospinning: recent advances and future prospects. *Chem Soc Rev* **2014**;*43*:4423.
32. Mercante LA, Scagion VP, Migliorini FL, Mattoso LHC, Correa DS. Electrospinning-based (bio)sensors for food and agricultural applications: a review. *Trac Trends Anal Chem* **2017**;*91*:91.
33. Li D, Wang YL, Xia YN. Electrospinning of polymeric and ceramic nanofibers as uniaxially aligned arrays. *Nano Lett* **2003**;*3*:1167.
34. Baji A, Mai YW, Wong SC, Abtahi M, Chen P. Electrospinning of polymer nanofibers: effects on oriented morphology, structures and tensile properties. *Compos Sci Technol* **2010**;*70*:703.
35. Agarwal S, Greiner A, Wendorff JH. Functional materials by electrospinning of polymers. *Prog Polym Sci* **2013**;*38*:963.
36. Ding YC, Hou HQ, Zhao Y, Zhu ZT, Fong H. Electrospun polyimide nanofibers and their applications. *Prog Polym Sci* **2016**;*61*:67.
37. Thakkar S, Misra M. Electrospun polymeric nanofibers: new horizons in drug delivery. *Eur J Pharm Sci* **2017**;*107*:148.
38. Bhardwaj N, Kundu SC. Electrospinning: a fascinating fiber fabrication technique. *Biotechnol Adv* **2010**;*28*:325.
39. Deitzel JM, Kleinmeyer J, Harris D, Tan NCB. The effect of processing variables on the morphology of electrospun nanofibers and textiles. *Polymer* **2001**;*42*:261.

40. Cheng J, Jun Y, Qin JH, Lee SH. Electrospinning versus microfluidic spinning of functional fibers for biomedical applications. *Biomaterials* **2017**;*114*:121.
41. Rutledge GC, Fridrikh SV. Formation of fibers by electrospinning. *Adv Drug Deliv Rev* **2007**;*59*:1384.
42. Frenot A, Chronakis IS. Polymer nanofibers assembled by electrospinning. *Curr Opin Colloid Interface Sci* **2003**;*8*:64.
43. Greiner A, Wendorff JH. Functional Self-Assembled Nanofibers by Electrospinning. In: Shimizu T, editor. Self-assembled nanomaterials I: nanofibers. Advances in Polymer Science, **2008**. p. 107.
44. Wang XM, Sun FZ, Yin GC, Wang YT, Liu B, Dong MD. Tactile-sensing based on flexible PVDF nanofibers via electrospinning: a review. *Sensors* **2018**;*18*:330.
45. Luo CJ, Stoyanov SD, Stride E, Pelan E, Edirisinghe M. Electrospinning versus fibre production methods: from specifics to technological convergence. *Chem Soc Rev* **2012**;*41*:4708.
46. Chen K, Chou WM, Liu LC, Cui YH, Xue P, Jia MY. Electrochemical sensors fabricated by electrospinning technology: an overview. *Sensors* **2019**;*19*:3676.
47. Reneker DH, Chun I. Nanometre diameter fibres of polymer, produced by electrospinning. *Nanotechnology* **1996**;*7*:216.
48. Mit-uppatham C, Nithitanakul M, Supaphol P. Ultratine electrospun polyamide-6 fibers: effect of solution conditions on morphology and average fiber diameter. *Macromol Chem Phys* **2004**;*205*:2327.
49. Saad EM, El Gohary NA, El-Shenawy BM, Handoussa H, Klingner A, Elwi M, Hamed Y, Khalil ISM, El Nashar RM, Mizaikoff B. Fabrication of magnetic molecularly imprinted beaded fibers for rosmarinic acid. *Nanomaterials* **2020**;*10*:1478.
50. Vicente A, Rivero PJ, Palacio JF, Rodriguez R. The role of the fiber/bead hierarchical microstructure on the properties of PVDF coatings deposited by electrospinning. *Polymers* **2021**;*13*:464.
51. Lee KH, Zhang SP, Lodge TP, Frisbie CD. Electrical impedance of spin-coatable ion gel films. *J Phys Chem B* **2011**;*115*:3315.
52. Schwartz G, Tee BCK, Mei JG, Appleton AL, Kim DH, Wang HL, Bao ZN. Flexible polymer transistors with high pressure sensitivity for application in electronic skin and health monitoring. *Nat Commun* **2013**;*4*:1859.
53. Fujimoto T, Awaga K. Electric-double-layer field-effect transistors with ionic liquids. *Phys Chem Chem Phys* **2013**;*15*:8983.
54. Nie BQ, Li RY, Cao J, Brandt JD, Pan TR. Flexible transparent iontronic film for interfacial capacitive pressure sensing. *Adv Mater* **2015**;*27*:6055.
55. Yuk H, Zhang T, Parada GA, Liu XY, Zhao XH. Skin-inspired hydrogel-elastomer hybrids with robust interfaces and functional microstructures. *Nat Commun* **2016**;*7*:12028.
56. Liu DP, Shi QQ, Jin S, Shao YL, Huang J. Self-assembled core-shell structured organic nanofibers fabricated by single-nozzle electrospinning for highly sensitive ammonia sensors. *Infomat* **2019**;*1*:525.
57. Chartuprayoon N, Zhang ML, Bosze W, Choa YH, Myung NV. One-dimensional nanostructures based bio-detection. *Biosens Bioelectron* **2015**;*63*:432.
58. Fan HJ, Gosele U, Zacharias M. Formation of nanotubes and hollow nanoparticles based on Kirkendall and diffusion processes: a review. *Small* **2007**;*3*:1660.
59. Liu RR, Hou LL, Yue GC, Li HK, Zhang JS, Liu J, Miao BB, Wang N, Bai J, Cui ZM, Liu TX, Zhao Y. Progress of fabrication and applications of electrospun hierarchically porous nanofibers. *Adv Fiber Mater* **2022**;*4*:604.
60. Xu F, Yang J, Dong RZ, Jiang HX, Wang CH, Liu WL, Jiang ZX, Zhang XQ, Zhu GD. Wave-shaped piezoelectric nanofiber membrane nanogenerator for acoustic detection and recognition. *Adv Fiber Mater* **2021**;*3*:368.
61. Kang SX, Zhao K, Yu DG, Zheng XL, Huang CX. Advances in biosensing and environmental monitoring based on electrospun nanofibers. *Adv Fiber Mater* **2022**;*4*:404.
62. Liu PC, Zhu YZ, Ma JH, Yang SG, Gong JH, Xu J. Preparation of continuous porous alumina nanofibers with hollow structure by single capillary electrospinning. *Colloids Surf Physicochem Eng Asp* **2013**;*436*:489.
63. Ma GP, Yang DZ, Nie J. Preparation of porous ultrafine polyacrylonitrile (PAN) fibers by electrospinning. *Polym Adv Technol* **2009**;*20*:147.
64. Scampicchio M, Arecchi A, Lawrence NS, Mannino S. Nylon nanofibrous membrane for mediated glucose biosensing. *Sens Actuators B Chem* **2010**;*145*:394.
65. Wanekaya AK, Chen W, Myung NV, Mulchandani A. Nanowire-based electrochemical biosensors. *Electroanalysis* **2006**;*18*:533.
66. Miller MR, Shaw CA, Langrish JP. From particles to patients: oxidative stress and the cardiovascular effects of air pollution. *Future Cardiol* **2012**;*8*:577.
67. Glencross DA, Ho TR, Camilla N, Hawrylowicz CM, Pfeffer PE. Air pollution and its effects on the immune system. *Free Radic Biol Med* **2020**;*151*:56.
68. Mahajan S, Jagtap S. Metal-oxide semiconductors for carbon monoxide (CO) gas sensing: a review. *Appl Mater Today* **2019**;*18*:100483.
69. Zhang ZB, Xue T, Jin XY. Effects of meteorological conditions and air pollution on COVID-19 transmission: evidence from 219 Chinese cities. *Sci Total Environ* **2020**;*741*:140244.
70. Mirzaei A, Leonardi SG, Neri G. Detection of hazardous volatile organic compounds (VOCs) by metal oxide nanostructures-based gas sensors: a review. *Ceram Int* **2016**;*42*:15119.
71. Kumar P, Deep A, Kim KH, Brown RJC. Coordination polymers: opportunities and challenges for monitoring volatile organic compounds. *Prog Polym Sci* **2015**;*45*:102.
72. Heft-Neal S, Burney J, Bendavid E, Burke M. Robust relationship between air quality and infant mortality in Africa. *Nature* **2018**;*559*:254.
73. Nikfarjam A, Hosseini S, Salehifar N. Fabrication of a highly sensitive single aligned TiO_2 and gold nanoparticle embedded TiO_2 nano-fiber gas sensor. *ACS Appl Mater Interfaces* **2017**;*9*:15662.
74. Su HY, Li H, Lin H, Shi XW, Du YM, Luo Y, Deng HB. Highly sensitive formaldehyde sensors based on CuO/ZnO composite nanofibrous mats using porous cellulose acetate fibers as templates. *Int J Biol Macromol* **2022**;*206*:653.
75. Wang N, Wang XF, Jia YT, Li XQ, Yu JY, Ding B. Electrospun nanofibrous chitosan membranes modified with polyethyleneimine for formaldehyde detection. *Carbohyd Polym* **2014**;*108*:192.
76. Zou YD, Zhou XR, Zhu YH, Cheng XW, Zhao DY, Deng YH. sp^2-Hybridized carbon-containing block copolymer templated synthesis of mesoporous semiconducting metal oxides with excellent gas sensing property. *Acc Chem Res* **2019**;*52*:714.
77. Ma JH, Ren Y, Zhou XR, Liu LL, Zhu YH, Cheng XW, Xu PC, Li XX, Deng YH, Zhao DY. Pt nanoparticles sensitized ordered mesoporous WO3 semiconductor: gas sensing performance and mechanism study. *Adv Funct Mater* **2018**;*28*:1705268.
78. Yang YR, Gao W. Wearable and flexible electronics for continuous molecular monitoring. *Chem Soc Rev* **2019**;*48*:1465.
79. Yao MS, Lv XJ, Fu ZH, Li WH, Deng WH, Wu GD, Xu G. Layer-by-layer assembled conductive metal-organic framework nanofilms for room-temperature chemiresistive sensing. *Angew Chem Int Ed* **2017**;*56*:16510.
80. Nasri A, Petrissans M, Fierro V, Celzard A. Gas sensing based on organic composite materials: review of sensor types, progresses and challenges. *Mater Sci Semicond Process* **2021**;*128*:105744.

81. Srinivasan P, Ezhilan M, Kulandaisamy AJ, Babu KJ, Rayappan JBB. Room temperature chemiresistive gas sensors: challenges and strategies—a mini review. *J Mater Sci Mater Electron* **2019**;*30*:15825.
82. Majhi SM, Mirzaei A, Kim HW, Kim SS, Kim TW. Recent advances in energy-saving chemiresistive gas sensors: a review. *Nano Energy* **2021**;*79*:105369.
83. UlAbideen Z, Kim JH, Lee JH, Kim JY, Mirzaei A, Kim HW, Kim SS. Electrospun metal oxide composite nanofibers gas sensors: a review. *J Korean Ceram Soc* **2017**;*54*:366.
84. Kim HJ, Lee JH. Highly sensitive and selective gas sensors using p-type oxide semiconductors: overview. *Sens Actuators B Chem* **2014**;*192*:607.
85. Xu HY, Ju DX, Chen ZR, Han R, Zhai T, Yu HQ, Liu CY, Wu XW, Wang JQ, Cao BQ. A novel hetero-structure sensor based on Au/Mg-doped TiO_2/SnO_2 nanosheets directly grown on Al_2O_3 ceramic tubes. *Sens Actuators B Chem* **2018**;*273*:328.
86. Wang C, Wang YL, Cheng PF, Xu LP, Dang F, Wang TL, Lei ZH. In-situ generated TiO_2/alpha-Fe_2O_3 heterojunction arrays for batch manufacturing of conductometric acetone gas sensors. *Sensors and Actuators B-Chemical*. **2021**, *340*.
87. Liang QH, Zou XX, Chen H, Fan MH, Li GD. High-performance formaldehyde sensing realized by alkaline-earth metals doped In_2O_3 nanotubes with optimized surface properties. *Sens Actuators B Chem* **2020**;*304*:127241.
88. Kou XY, Meng FQ, Chen K, Wang TS, Sun P, Liu FM, Yan X, Sun YF, Liu FM, Shimanoe K, Lu GY. High-performance acetone gas sensor based on Ru-doped SnO_2 nanofibers. *Sens Actuators B Chem* **2020**;*320*:128292.
89. Trung TQ, Duy LT, Ramasundaram S, Lee NE. Transparent, stretchable, and rapid-response humidity sensor for body-attachable wearable electronics. *Nano Res* **2021**;*2017*:10.
90. Han CH, Li XW, Shao CL, Li XH, Ma JG, Zhang XT, Liu YC. Composition-controllable p-CuO/n-ZnO hollow nanofibers for high-performance H2S detection. *Sens Actuators B Chem* **2019**;*285*:495.
91. Zhang R, Cao S, Zhou TT, Fei T, Wang R, Zhang T. Rational design and tunable synthesis of Co3O4 nanoparticle-incorporating into In_2O_3 one-dimensional ribbon as effective sensing material for gas detection. *Sens Actuators B Chem* **2020**;*310*:127695.
92. Li XW, Han CH, Lu DX, Shao CL, Li XH, Liu YC. Highly electron-depleted ZnO/$ZnFe_2O_4$/Au hollow meshes as an advanced material for gas sensing application. *Sens Actuators B Chem* **2019**;*297*:126769.
93. Zhang M, Sui N, Wang R, Zhang T. The effect of shell thickness on gas sensing properties of core-shell fibers. *Sens Actuators B Chem* **2021**;*332*:129456.
94. Filippidou MK, Chatzichristidi M, Chatzandroulis S. A fabrication process of flexible IDE capacitive chemical sensors using a two step lift-off method based on PVA patterning. *Sens Actuators B Chem* **2019**;*284*:7.
95. Rivadeneyra A, Fernandez-Salmeron J, Banqueri J, Lopez-Villanueva JA, Capitan-Vallvey LF, Palma AJ. A novel electrode structure compared with interdigitated electrodes as capacitive sensor. *Sens Actuators B Chem* **2014**;*204*:552.
96. Bulemo PM, Kim DH, Kim ID. Controlled synthesis of electrospun hollow Pt-loaded SnO_2 microbelts for acetone sensing. *Sens Actuators B Chem* **2021**;*344*:130208.
97. Zhao LB, Zhao YH, Xia Y, Li ZK, Li J, Zhang JW, Wang JH, Zhou XY, Li YJ, Zhao YL, Jiang ZD. A novel CMUT-based resonant biochemical sensor using electrospinning technology. *IEEE Trans Ind Electron* **2019**;*66*:7356.
98. Bai X, Lv H, Liu Z, Chen JK, Wang J, Sun BH, Zhang Y, Wang RH, Shi KY. Thin-layered MoS_2 nanoflakes vertically grown on SnO2 nanotubes as highly effective room-temperature NO_2 gas sensor. *J Hazard Mater* **2021**;*416*:125830.
99. Zhao DW, Zhu Y, Cheng WK, Chen WS, Wu YQ, Yu HP. Cellulose-based flexible functional materials for emerging intelligent electronics. *Adv Mater* **2021**;*33*:2000619.
100. Yang LY, Xu XR, Liu MD, Chen C, Cui J, Chen X, Wu K, Sun DP. Wearable and flexible bacterial cellulose/polyaniline ammonia sensor based on a synergistic doping strategy. *Sens Actuators B Chem* **2021**;*334*:129647.
101. Zhu ZY, Liu CC, Jiang FX, Liu J, Liu GQ, Ma XM, Liu PP, Huang R, Xu JK, Wang L. Flexible fiber-shaped hydrogen gas sensor via coupling palladium with conductive polymer gel fiber. *J Hazard Mater* **2021**;*411*:125008.
102. Nair KG, Vishnuraj R, Pullithadathil B. Highly sensitive, flexible H_2 gas sensors based on less platinum bimetallic Ni-Pt nanocatalyst-functionalized carbon nanofibers. *ACS Appl Electron Mater* **2021**;*3*:1621.
103. Khalifa M, Anandhan S. Highly sensitive and wearable NO_2 gas sensor based on PVDF nanofabric containing embedded polyaniline/g-C_3N_4 nanosheet composites. *Nanotechnology* **2021**;*32*:485504.
104. Guo CX, Sedgwick AC, Hirao T, Sessler JL. Supramolecular fluorescent sensors: an historical overview and update. *Coord Chem Rev* **2021**;*427*:213560.
105. Wu Z, Liu MM, Liu ZC, Tian Y. Real-time imaging and simultaneous quantification of mitochondrial H_2O_2 and ATP in neurons with a single two-photon fluorescence-lifetime-based probe. *J Am Chem Soc* **2020**;*142*:7532.
106. Tavakoli J, Pye S, Reza A, Xie N, Qin J, Raston CL, Tang BZ, Tang YH. Tuning aggregation-induced emission nanoparticle properties under thin film formation. *Mater Chem Front* **2020**;*4*:537.
107. Feng HT, Yuan YX, Xiong JB, Zheng YS, Tang BZ. Macrocycles and cages based on tetraphenylethylene with aggregation-induced emission effect. *Chem Soc Rev* **2018**;*47*:7452.
108. Li DD, Yu JH. AIEgens-functionalized inorganic-organic hybrid materials: fabrications and applications. *Small* **2016**;*12*:6478.
109. Tavakoli J, Gascooke J, Xie N, Tang B, Tang YH. Enlightening freeze thaw process of physically cross-linked poly(vinyl alcohol) hydrogels by aggregation-induced emission fluorogens. *Acs Appl Polym Mater* **2019**;*1*:1390.
110. Gao M, Xu GC, Zhang RH, Liu ZJ, Xia HM, Shao B, Xue CH, Li JC, Miao SH, Fu WL, Zhang XS, Zhou JJ, Jiang XP, Liang K, Kong B. Electrospinning superassembled mesoporous AlEgen-organosilica frameworks featuring diversified forms and superstability for wearable and washable solid-state fluorescence smart sensors. *Anal Chem* **2021**;*93*:2367.
111. Mao YY, Akram M, Shi JY, Wen JX, Yang C, Jiang JP, Lu ZG, Zhou BP, Tian YQ. Optical oxygen sensors based on microfibers formed from fluorinated copolymers. *Sens Actuators B Chem* **2019**;*282*:885.
112. Zhang K, Luo LL, Li WJ, Zhang HL, Zhang Y, Zhao JP, Li Y. High-performance dissolved oxygen sensors based on platinum(II) porphyrin embedded in polystyrene beads. *New J Chem* **2017**;*41*:6646.
113. Mao YY, Zhao Q, Wu JC, Pan TT, Zhou BP, Tian YQ. A highly sensitive and fast-responding oxygen sensor based on POSS-containing hybrid copolymer films. *J Mater Chem C* **2017**;*5*:11395.
114. Sun ZJ, Cai CX, Guo F, Ye CH, Luo YW, Ye SM, Luo JC, Zhu F, Jiang CY. Oxygen sensitive polymeric nanocapsules for optical dissolved oxygen sensors. *Nanotechnology* **2018**;*29*:145704.
115. Huang TC, Yeh LC, Lai GH, Huang BS, Yang TI, Hsu SC, Lo AY, Yeh JM. Advanced superhydrophobic electroactive fluorinated polyimide and its application in anticorrosion coating. *Int J Green Energy* **2017**;*14*:113.
116. Ren K, Wang J, Jia HL. Electrospinning fibrous films doped with iridium complexes for high performance oxygen sensing: synthesis and characterization. *Sens Actuators B Chem* **2017**;*240*:697.

117. Cavaliere S, Subianto S, Savych I, Jones DJ, Roziere J. Electrospinning: designed architectures for energy conversion and storage devices. *Energy Environ Sci* **2011**;*4*:4761.
118. Zaitsev NK, Melnikov PV, Alferov VA, Kopytin AV, German KE, editors. Stable optical oxygen sensing material based on perfluorinated polymer and fluorinated platinum(II) and palladium(II) porphyrins. 30th Eurosensors Conference; 2016 Sep 04–07; Budapest, HUNGARY; **2016**.
119. Estella J, Wencel D, Moore JP, Sourdaine M, McDonagh C. Fabrication and performance evaluation of highly sensitive hybrid sol-gel-derived oxygen sensor films based on a fluorinated precursor. *Anal Chim Acta* **2010**;*666*:83.
120. Mao YY, Mei ZP, Wen JY, Li G, Tian YH, Zhou BP, Tian YQ. Honeycomb structured porous films from a platinum porphyrin-grafted poly(styrene-co-4-vinylpyridine) copolymer as an optical oxygen sensor. *Sens Actuators B Chem* **2018**;*257*:944.
121. Schoolaert E, Hoogenboom R, De Clerck K. Colorimetric nanofibers as optical sensors. *Adv Funct Mater* **2017**;*27*:1702646.
122. Lagerwall JPF, McCann JT, Formo E, Scalia G, Xia YN. Coaxial electrospinning of microfibres with liquid crystal in the core. *Chem Commun* **2008**;*42*:5420–5422.
123. Wang JR, Jakli A, West JL. Morphology tuning of electrospun liquid crystal/polymer fibers. *ChemPhysChem* **2016**;*17*:3080.
124. Wang D, Park SY, Kang IK. Liquid crystals: emerging materials for use in real-time detection applications. *J Mater Chem C* **2015**;*3*:9038.
125. Cadwell KD, Lockwood NA, Nellis BA, Alf ME, Willis CR, Abbott NL. Detection of organophosphorous nerve agents using liquid crystals supported on chemically functionalized surfaces. *Sens Actuators B Chem* **2007**;*128*:91.
126. Reyes CG, Sharma A, Lagerwall JPF. Non-electronic gas sensors from electrospun mats of liquid crystal core fibres for detecting volatile organic compounds at room temperature. *Liq Cryst* **1986**;*2016*:43.
127. Wang JR, Jakli A, West JL. Liquid crystal/polymer fiber mats as sensitive chemical sensors. *J Mol Liq* **2018**;*267*:490.
128. Agra-Kooijman DM, Robb C, Guan Y, Jakli A, West JL. Liquid crystal core polymer fiber mat electronic gas sensors. *Liq Cryst* **2021**;*48*:1880–1887.
129. Cha JH, Kim DH, Choi SJ, Koo WT, Kim ID. Sub-parts-per-million hydrogen sulfide colorimetric sensor: lead acetate anchored nanofibers toward halitosis diagnosis. *Anal Chem* **2018**;*90*:8769.
130. Cha XL, Yu FF, Fan Y, Chen JF, Wang LY, Xiang Q, Duan ZM, Xu JQ. Superhydrophilic ZnO nanoneedle array: controllable in situ growth on QCM transducer and enhanced humidity sensing properties and mechanism. *Sens Actuators B Chem* **2018**;*263*:436.
131. Wang LY, Zhu Y, Xiang Q, Cheng ZX, Chen Y, Xu JQ. One novel humidity-resistance formaldehyde molecular probe based hydrophobic diphenyl sulfone urea dry-gel: synthesis, sensing performance and mechanism. *Sens Actuators B Chem* **2017**;*251*:590.
132. Wang LY. Metal-organic frameworks for QCM-based gas sensors: a review. *Sens Actuators A Phys* **2020**;*307*:11984.
133. Boyadjiev SI, Georgieva V, Stefan N, Stan GE, Mihailescu N, Visan A, Mihailescu IN, Besleaga C, Szilagyi IM. Characterization of PLD grown WO_3 thin films for gas sensing. *Appl Surf Sci* **2017**;*417*:218.
134. Wang LY, Xu J, Wang XH, Cheng ZX, Xu JQ. Facile preparation of N-rich functional polymer with porous framework as QCM sensing material for rapid humidity detection. *Sens Actuators B Chem* **2019**;*288*:289.
135. Yang MQ, He JH. Graphene oxide as quartz crystal microbalance sensing layers for detection of formaldehyde. *Sens Actuators B Chem* **2016**;*228*:486.
136. Kang ZJ, Zhang DZ, Li TT, Liu XH, Song XS. Polydopamine-modified SnO_2 nanofiber composite coated QCM gas sensor for high-performance formaldehyde sensing. *Sens Actuators B Chem* **2021**;*345*:130299.
137. Yang MQ, He JH. A copper-manganese composite oxide as QCM sensing layers for detection of formaldehyde gas. *RSC Adv* **2018**;*8*:22.
138. Wang LY, Yu YP, Xiang Q, Xu J, Cheng ZX, Xu JQ. PODS-covered PDA film based formaldehyde sensor for avoiding humidity false response. *Sens Actuators B Chem* **2018**;*255*:2704.
139. El Yakhlifi S, Ball V. Polydopamine as a stable and functional nanomaterial. *Colloids Surf B Biointerfaces* **2020**;*186*:110719.
140. Zong J, Zhang YS, Zhu Y, Zhao Y, Zhang WJ, Zhu YH. Rapid and highly selective detection of formaldehyde in food using quartz crystal microbalance sensors based on biomimetic polydopamine functionalized hollow mesoporous silica spheres. *Sens Actuators B Chem* **2018**;*271*:311.
141. Diltemiz SE, Ecevit K. High-performance formaldehyde adsorption on CuO/ZnO composite nanofiber coated QCM sensors. *J Alloy Compd* **2019**;*783*:608.
142. Zhang HD, Yan X, Zhang ZH, Yu GF, Han WP, Zhang JC, Long YZ. Electrospun PEDOT: PSS/PVP nanofibers for CO gas sensing with quartz crystal microbalance technique. *Int J Polym Sci*. **2016**, *2016*.
143. Nagajyoti PC, Lee KD, Sreekanth TVM. Heavy metals, occurrence and toxicity for plants: a review. *Environ Chem Lett* **2010**;*8*:199.
144. Kumar V, Parihar RD, Sharma A, Bakshi P, Sidhu GPS, Bali AS, Karaouzas L, Bhardwaj R, Thukral AK, Gyasi-Agyei Y, Rodrigo-Comino J. Global evaluation of heavy metal content in surface water bodies: a meta-analysis using heavy metal pollution indices and multivariate statistical analyses. *Chemosphere* **2019**;*236*:124364.
145. Vardhan KH, Kumar PS, Panda RC. A review on heavy metal pollution, toxicity and remedial measures: current trends and future perspectives. *J Mol Liq* **2019**;*290*:111197.
146. Malik LA, Bashir A, Qureashi A, Pandith AH. Detection and removal of heavy metal ions: a review. *Environ Chem Lett* **2019**;*17*:1495–1521.
147. Peters GR, McCurdy RF, Hindmarsh JT. Environmental aspects of arsenic toxicity. *Crit Rev Clin Lab Sci* **1996**;*33*:457.
148. Liu YC, Tian X, Cao SW, Li Y, Dong HJ, Li YS. Pollution characteristics and health risk assessment of arsenic transformed from feed additive organoarsenicals around chicken farms on the North China Plain. *Chemosphere* **2021**;*278*:130438.
149. Liu YH, Xue Q, Chang CW, Wang R, Wang Q, Shan XH. Highly efficient detection of Cd(II) ions by a stannum and cerium bimetal-modified laser-induced graphene electrode in water. *Chem Eng J* **2022**;*433*:133791.
150. Yi YH, Zhao Y, Zhang ZM, Wu YT, Zhu GB. Recent developments in electrochemical detection of cadmium. *Trends Environ Anal Chem* **2022**;*33*:e00152.
151. Wang CY, Ma SJ, Pan L, Wu WR, Wei YM, Ou JJ. Cyclized conjugated microporous polymer-coated silica nanospheres as fluorescent sensors for iron(III) and chromium(III). *Chem Eng J* **2022**;*435*:134368.
152. Wang GQ, Zhang SR, Cui JZ, Gao WS, Rong X, Lu YX, Gao CZ. Preparation of nitrogen-doped carbon quantum dots from chelating agent and used as fluorescent probes for accurate detection of ClO- and Cr(VI). *Anal Chim Acta* **2022**;*1195*:339478.
153. Xu JM, Liu MB, Zhao WH, Wang SQ, Gui MF, Li HB, Yu RQ. DNAzyme-based cascade signal amplification strategy for highly sensitive detection of lead ions in the environment. *J Hazard Mater* **2022**;*429*:128347.
154. Shu Y, Ye QY, Dai T, Guan J, Ji ZP, Xu Q, Hu XY. Incorporation of perovskite nanocrystals into lanthanide metal-organic

frameworks with enhanced stability for ratiometric and visual sensing of mercury in aqueous solution. *J Hazard Mater* **2022**;*430*:128360.
155. Stala L, Ulatowska J, Polowczyk I. A review of polyampholytic ion scavengers for toxic metal ion removal from aqueous systems. *Water Res* **2021**;*203*:117523.
156. Gong ZD, Lei YS, Wang ZW, Zhang J, Sun ZJ, Li YY, Huang JH, Chan CC, Ouyang X. A taper-in-taper structured interferometric optical fiber sensor for Cu^{2+} ion detection. *Sensors* **2022**;*22*:2709.
157. Leung AOW, Duzgoren-Aydin NS, Cheung KC, Wong MH. Heavy metals concentrations of surface dust from e-waste recycling and its human health implications in southeast China. *Environ Sci Technol* **2008**;*42*:2674.
158. Gomes SIL, de Boer TE, van Gestel CAM, van Straalen NM, Soares A, Roelofs D, Amorim MJB. Molecular mechanisms of zinc toxicity in the potworm Enchytraeus crypticus, analysed by high-throughput gene expression profiling. *Sci Total Environ* **2022**;*825*:153975.
159. Naveen MH, Gurudatt NG, Shim YB. Applications of conducting polymer composites to electrochemical sensors: a review. *Appl Mater Today* **2017**;*9*:419.
160. Kuila T, Bose S, Khanra P, Mishra AK, Kim NH, Lee JH. Recent advances in graphene-based biosensors. *Biosens Bioelectron* **2011**;*26*:4637.
161. Promphet N, Rattanarat P, Rangkupan R, Chailapakul O, Rodthongkum N. An electrochemical sensor based on graphene/polyaniline/polystyrene nanoporous fibers modified electrode for simultaneous determination of lead and cadmium. *Sens Actuators B Chem* **2015**;*207*:526.
162. Huang H, Zhu WC, Gao XC, Liu XY, Ma HY. Synthesis of a novel electrode material containing phytic acid-polyaniline nanofibers for simultaneous determination of cadmium and lead ions. *Anal Chim Acta* **2016**;*947*:32.
163. Zhao DL, Wang TT, Han D, Rusinek C, Steckl AJ, Heineman WR. Electrospun carbon nanofiber modified electrodes for stripping voltammetry. *Anal Chem* **2015**;*87*:9315.
164. Gao SS, Liu J, Luo J, Mamat X, Sambasivam S, Li YT, Hu X, Wagberg T, Hu GZ. Selective voltammetric determination of Cd(II) by using N, S-codoped porous carbon nanofibers. *Microchim Acta* **2018**;*185*:282.
165. Tang Q, Zhu GD, Ge YX, Yang JM, Huang MH, Liu JY. AuNPs-polyaniline nanosheet array on carbon nanofiber for the determination of As(III). *J Electroanal Chem* **2020**;*873*:114381.
166. Yu XY, Liu ZG, Huang XJ. Nanostructured metal oxides/hydroxides-based electrochemical sensor for monitoring environmental micropollutants. *Trends Environ Anal Chem* **2014**;*3–4*:28.
167. Oliveira VHB, Rechotnek F, da Silva EP, Marques VD, Rubira AF, Silva R, Lourenco SA, Muniz EC. A sensitive electrochemical sensor for Pb^{2+} ions based on ZnO nanofibers functionalized by L-cysteine. *J Mol Liq* **2020**;*309*:113041.
168. Girija S, Sankar SS, Thenrajan T, Kundu S, Wilson J. Bi-metallic zeolite imidazole framework nanofibers for the selective determination of Cd^{2+} ions. *J Mater Chem B* **2021**;*9*:5656.
169. Teodoro KBR, Shimizu FM, Scagion VP, Correa DS. Ternary nanocomposites based on cellulose nanowhiskers, silver nanoparticles and electrospun nanofibers: use in an electronic tongue for heavy metal detection. *Sens Actuators B Chem* **2019**;*290*:387.
170. Li ZX, Li HX, Shi CX, Zhang WY, Zhou W, Wei LH, Yu MM. Naked-eye-based highly selective sensing of Fe^{3+} and further for PPi with nano copolymer film. *Sens Actuators B Chem* **2016**;*226*:127.
171. Abedalwafa MA, Li Y, Li D, Sanbhal N, Yang JM, Wang L. Aminated polyacrylonitrile nanofibers with immobilized gold-silver core-shell nanoparticles for use in a colorimetric test strip for copper(II). *Microchim Acta* **2018**;*185*:402
172. Zhang CD, Li HD, Yu QZ, Jia L, Wan LY. Poly(aspartic acid) electrospun nanofiber hydrogel membrane-based reusable colorimetric sensor for Cu(II) and Fe(III) detection. *ACS Omega* **2019**;*4*:14633.
173. Wang L, Li M, Li WT, Han Y, Liu YJ, Li Z, Zhang BH, Pan DY. Rationally designed efficient dual-mode colorimetric/fluorescence sensor based on carbon dots for detection of pH and Cu^{2+} Ions. *Acs Sustain Chem Eng* **2018**;*6*:12668.
174. Terra IAA, Mercante LA, Andre RS, Correa DS. Fluorescent and colorimetric electrospun nanofibers for heavy-metal sensing. *Biosensors (Basel)* **2017**;*7*:61.
175. Hu Y, Chen L, Jung H, Zeng YY, Lee S, Swamy KMK, Zhou X, Kim MH, Yoon J. Effective strategy for colorimetric and fluorescence sensing of phosgene based on small organic dyes and nanofiber platforms. *ACS Appl Mater Interfaces* **2016**;*8*:22246.
176. Wang W, Li YP, Sun MD, Zhou C, Zhang Y, Li YX, Yang QB. Colorimetric and fluorescent nanofibrous film as a chemosensor for Hg^{2+} in aqueous solution prepared by electrospinning and host-guest interaction. *Chem Commun* **2012**;*48*:6040.
177. Parsaee Z. Electrospun nanofibers decorated with bio-sonochemically synthesized gold nanoparticles as an ultrasensitive probe in amalgam-based mercury(II) detection system. *Ultrason Sonochem* **2018**;*44*:24.
178. Guo PZ, Sikdar D, Huang XQ, Si KJ, Xiong W, Gong S, Yap LW, Premaratne M, Cheng WL. Plasmonic core-shell nanoparticles for SERS detection of the pesticide thiram: size- and shape-dependent Raman enhancement. *Nanoscale* **2015**;*7*:2862.
179. Yang T, Ma J, Zhen SJ, Huang CZ. Electrostatic assemblies of well-dispersed AgNPs on the surface of electrospun nanofibers as highly active SERS substrates for wide range pH sensing. *ACS Appl Mater Interfaces* **2016**;*8*:14802.
180. Xu SY, Tang WQ, Chase DB, Sparks DL, Rabolt JF. A Highly sensitive, selective, and reproducible SERS sensor for detection of trace metalloids in the environment. *Acs Appl Nano Mater* **2018**;*1*:1257.
181. Zhang H, Cao MH, Wu W, Xu HB, Cheng S, Fan LJ. Polyacrylonitrile/noble metal/SiO_2 nanofibers as substrates for the amplified detection of picomolar amounts of metal ions through plasmon-enhanced fluorescence. *Nanoscale* **2015**;*7*:1374.
182. Wang Q, Xue Q, Chen T, Li JW, Liu YH, Shan XH, Liu F, Jia JB. Recent advances in electrochemical sensors for antibiotics and their applications. *Chin Chem Lett* **2021**;*32*:609.
183. Sun SM, Korheina DKA, Fu HT, Ge XP. Chronic exposure to dietary antibiotics affects intestinal health and antibiotic resistance gene abundance in oriental river prawn (Macrobrachium nipponense), and provokes human health risk. *Sci Total Environ* **2020**;*720*:137478.
184. Kumar M, Jaiswal S, Sodhi KK, Shree P, Singh DK, Agrawal PK, Shukla P. Antibiotics bioremediation: perspectives on its ecotoxicity and resistance. *Environ Int* **2019**;*124*:448.
185. Huang FY, An ZY, Moran MJ, Liu F. Recognition of typical antibiotic residues in environmental media related to groundwater in China (2009–2019). *J Hazard Mater* **2020**;*399*:122813.
186. Wang HX, Wang N, Wang B, Zhao Q, Fang H, Fu CW, Tang CX, Jiang F, Zhou Y, Chen Y, Jiang QW. Antibiotics in drinking water in Shanghai and their contribution to antibiotic exposure of school children. *Environ Sci Technol* **2016**;*50*:2692.
187. Qiao M, Ying GG, Singer AC, Zhu YG. Review of antibiotic resistance in China and its environment. *Environ Int* **2018**;*110*:160.
188. Yang YY, Song WJ, Lin H, Wang WB, Du LN, Xing W. Antibiotics and antibiotic resistance genes in global lakes: a review and meta-analysis. *Environ Int* **2018**;*116*:60.
189. Zhang QQ, Ying GG, Pan CG, Liu YS, Zhao JL. Comprehensive evaluation of antibiotics emission and fate in the river Basins

of China: source analysis, multimedia modeling, and linkage to bacterial resistance. *Environ Sci Technol* **2015**;*49*:6772.
190. Ying GG, He LY, Ying AJ, Zhang QQ, Liu YS, Zhao JL. China must reduce its antibiotic use. *Environ Sci Technol* **2017**;*51*:1072.
191. Bu QW, Wang B, Huang J, Deng SB, Yu G. Pharmaceuticals and personal care products in the aquatic environment in China: a review. *J Hazard Mater* **2013**;*262*:189.
192. Huang FY, Zou SZ, Deng DD, Lang H, Liu F. Antibiotics in a typical karst river system in China: spatiotemporal variation and environmental risks. *Sci Total Environ* **2019**;*650*:1348.
193. Liu X, Steele JC, Meng XZ. Usage, residue, and human health risk of antibiotics in Chinese aquaculture: a review. *Environ Pollut* **2017**;*223*:161.
194. Li S, Shi WZ, Liu W, Li HM, Zhang W, Hu JR, Ke YC, Sun WL, Ni JR. A duodecennial national synthesis of antibiotics in China's major rivers and seas (2005–2016). *Sci Total Environ* **2018**;*615*:906.
195. Baby JN, Sriram B, Wang SF, George M. Integration of samarium vanadate/carbon nanofiber through synergy: an electrochemical tool for sulfadiazine analysis. *J Hazard Mater* **2021**;*408*:124940.
196. Song JL, Huang MH, Lin XH, Li SFY, Jiang N, Liu YB, Guo HD, Li YM. Novel Fe-based metal-organic framework (MOF) modified carbon nanofiber as a highly selective and sensitive electrochemical sensor for tetracycline detection. *Chem Eng J* **2022**;*427*:130913.
197. Ayankojo AG, Reut J, Opik A, Furchner A, Syritski V. Hybrid molecularly imprinted polymer for amoxicillin detection. *Biosens Bioelectron* **2018**;*118*:102.
198. Yang GM, Zhao FQ. Molecularly imprinted polymer grown on multiwalled carbon nanotube surface for the sensitive electrochemical determination of amoxicillin. *Electrochim Acta* **2015**;*174*:33.
199. Chen CL, Lv XC, Lei W, Wu Y, Feng SS, Ding Y, Lv JJ, Hao QL, Chen SM. Amoxicillin on polyglutamic acid composite three-dimensional graphene modified electrode: reaction mechanism of amoxicillin insights by computational simulations. *Anal Chim Acta* **2019**;*1073*:22.
200. Zhang Y, Tang WF, Wang YQ, Nian M, Jiang F, Zhang J, Chen Q. Environmental antibiotics exposure in school-age children in Shanghai and health risk assessment: a population-based representative investigation. *Sci Total Environ* **2022**;*824*:153859.
201. Wang HX, Yang JQ, Yu X, Zhao GM, Zhao Q, Wang N, Jiang YG, Jiang F, He GS, Chen Y, Zhou ZJ, Jiang QW. Exposure of adults to antibiotics in a shanghai suburban area and health risk assessment: a biomonitoring-based study. *Environ Sci Technol* **2018**;*52*:13942.
202. Tan XQ, Liang YP, Ye YY, Liu ZH, Meng JX, Li FY. Explainable deep learning-assisted fluorescence discrimination for aminoglycoside antibiotic identification. *Anal Chem* **2022**;*94*:829–836.
203. Pan Y, Shan D, Ding LL, Yang XD, Xu K, Huang H, Wang JF, Ren HQ. Developing a generally applicable electrochemical sensor for detecting macrolides in water with thiophene-based molecularly imprinted polymers. *Water Res* **2021**;*205*:117670.
204. Omuferen LO, Maseko B, Olowoyo JO. Occurrence of antibiotics in wastewater from hospital and convectional wastewater treatment plants and their impact on the effluent receiving rivers: current knowledge between 2010 and 2019. *Environ Monit Assess* **2022**;*194*:306.
205. Yin Y, Zhu D, Yang G, Su JQ, Duan GL. Diverse antibiotic resistance genes and potential pathogens inhabit in the phyllosphere of fresh vegetables. *Sci Total Environ* **2022**;*815*:152851.
206. Wang J, Teng XM, Wang YS, Si SX, Ju J, Pan W, Wang JP, Sun XB, Wang WJ. Carbon dots based fluorescence methods for the detections of pesticides and veterinary drugs: response mechanism, selectivity improvement and application. *Trac-Trends Anal Chem* **2021**;*144*:116430.
207. Bu F, Huang W, Xian M, Zhang XL, Liang FB, Liu XC, Sun XY, Feng DX. Magnetic carboxyl-functionalized covalent organic frameworks for adsorption of quinolones with high capacities, fast kinetics and easy regeneration. *J Clean Prod* **2022**;*336*:130485.
208. Wang HX, Wang N, Wang B, Fang H, Fu CW, Tang CX, Jiang F, Zhou Y, He GS, Zhao Q, Chen Y, Jiang QW. Antibiotics detected in urines and adipogenesis in school children. *Environ Int* **2016**;*89–90*:204.
209. Liu ZP, Jin ML, Lu H, Yao JY, Wang X, Zhou GF, Shui LL. Molecularly imprinted polymer decorated 3D-framework of functionalized multi-walled carbon nanotubes for ultrasensitive electrochemical sensing of Norfloxacin in pharmaceutical formulations and rat plasma. *Sens Actuators B Chem* **2019**;*288*:363.
210. Feng LM, Xue Q, Liu F, Cao QP, Feng JJ, Yang L, Zhang FL. Voltammetric determination of ofloxacin by using a laser-modified carbon glassy electrode. *Microchim Acta* **2020**;*187*:86.
211. Fenzl C, Nayak P, Hirsch T, Wolfbeis OS, Alshareef HN, Baeumner AJ. Laser-scribed graphene electrodes for aptamer-based biosensing. *Acs Sens* **2017**;*2*:616.
212. Starzec K, Cristea C, Tertis M, Feier B, Wieczorek M, Koscielniak P, Kochana J. Employment of electrostriction phenomenon for label-free electrochemical immunosensing of tetracycline. *Bioelectrochemistry* **2020**;*132*:107405.
213. Ni Y, Liao Y, Zheng MB, Shao SJ. In-situ growth of Co_3O_4 nanoparticles on mesoporous carbon nanofibers: a new nanocomposite for nonenzymatic amperometric sensing of H_2O_2. *Microchim Acta* **2017**;*184*:3689.
214. Kokulnathan T, Sharma TSK, Chen SM, Han-Yu Y. Synthesis and characterization of zirconium dioxide anchored carbon nanofiber composite for enhanced electrochemical determination of chloramphenicol in food samples. *J Electrochem Soc* **2018**;*165*:B281.
215. Qin LY, Yang DZ, Zhang M, Zhao TY, Luo Z, Yu ZZ. Superelastic and ultralight electrospun carbon nanofiber/MXene hybrid aerogels with anisotropic microchannels for pressure sensing and energy storage. *J Colloid Interface Sci* **2021**;*589*:264.
216. Scagion VP, Mercante LA, Sakamoto KY, Oliveira JE, Fonseca FJ, Mattoso LHC, Ferreira MD, Correa DS. An electronic tongue based on conducting electrospun nanofibers for detecting tetracycline in milk samples. *RSC Adv* **2016**;*6*:103740.
217. Chen XY, Hao SB, Zong BY, Liu CB, Mao S. Ultraselective antibiotic sensing with complementary strand DNA assisted aptamer/MoS_2 field-effect transistors. *Biosens Bioelectron* **2019**;*145*:111711.
218. Yin XH, Hou T, Huang BZ, Yang LM, Li F. Aptamer recognition-trigged label-free homogeneous electrochemical strategy for an ultrasensitive cancer-derived exosome assay. *Chem Commun* **2019**;*55*:13705.
219. Li FL, Wang XY, Sun X, Guo YM. Multiplex electrochemical aptasensor for detecting multiple antibiotics residues based on carbon fiber and mesoporous carbon-gold nanoparticles. *Sens Actuators B Chem* **2018**;*265*:217.
220. Ramezani M, Danesh NM, Lavaee P, Abnous K, Taghdisi SM. A selective and sensitive fluorescent aptasensor for detection of kanamycin based on catalytic recycling activity of exonuclease III and gold nanoparticles. *Sens Actuators B Chem* **2016**;*222*:1.
221. Yang Y, Yang ZH, Lv JJ, Yuan R, Chai YQ. Thrombin aptasensor enabled by Pt nanoparticles-functionalized Co-based metal organic frameworks assisted electrochemical signal amplification. *Talanta* **2017**;*169*:44.
222. Lebedev OI, Millange F, Serre C, Van Tendeloo G, Ferey G. First direct imaging of giant pores of the metal-organic framework MIL-101. *Chem Mater* **2005**;*17*:6525.
223. Liu Z, Su RD, Sun X, Zhou WZ, Gao BY, Yue QY, Li Q. The obvious advantage of amino-functionalized metal-organic

frameworks: as a persulfate activator for bisphenol F degradation. *Sci Total Environ* **2020**;*741*:140464.
224. Vafaye SE, Rahman A, Safaeian S, Adabi M. An electrochemical aptasensor based on electrospun carbon nanofiber mat and gold nanoparticles for the sensitive detection of Penicillin in milk. *J Food Meas Charact* **2021**;*15*:876.
225. Liu Q, Zheng YM, Zhong LB, Cheng XX. Removal of tetracycline from aqueous solution by a Fe_3O_4 incorporated PAN electrospun nanofiber mat. *J Environ Sci* **2015**;*28*:29.
226. Mudabuka B, Ogunlaja AS, Tshentu ZR, Torto N. Electrospun poly(vinylbenzyl chloride) nanofibres functionalised with tris-(2,2′-pyridylimidazole)iron(III): a test strip for detection of ascorbic acid and dopamine. *Sens Actuators B Chem* **2016**;*222*:598.
227. Li Y, Mohammed A, Li D, Wang L. Test strips based on iron(III)-impregnated alginate/polyacrylonitrile nanofibers for naked eye screening of tetracycline. *Analyst* **2018**;*143*:3029.
228. Chen D, Deng J, Liang J, Xie J, Hu CH, Huang KH. A core-shell molecularly imprinted polymer grafted onto a magnetic glassy carbon electrode as a selective sensor for the determination of metronidazole. *Sens Actuators B Chem* **2013**;*183*:594.
229. Abedalwafa MA, Li Y, Ni CF, Yang G, Wang L. Non-enzymatic colorimetric sensor strip based on melamine-functionalized gold nanoparticles assembled on polyamide nanofiber membranes for the detection of metronidazole. *Anal Methods* **2019**;*11*:3706.
230. Mao K, Yang ZG, Zhang H, Li XQ, Cooper JM. Paper-based nanosensors to evaluate community-wide illicit drug use for wastewater-based epidemiology. *Water Res* **2021**;*189*:116559.
231. Tang YZ, Chen X, Lv Y, Wu ZY, Chen F, Chen ZG. Excellent surface enhanced raman scattering of SiO_2 fiber membrane embedded with Ag nanoparticles. *J Inorg Organomet Polym Mater* **2018**;*28*:251.
232. Supraja P, Tripathy S, Vanjari SRK, Singh V, Singh SG. Electrospun tin (IV) oxide nanofiber based electrochemical sensor for ultra-sensitive and selective detection of atrazine in water at trace levels. *Biosens Bioelectron* **2019**;*141*:111441.
233. Yang XM, Li X, Zhang LZ, Gong JM. Electrospun template directed molecularly imprinted nanofibers incorporated with BiOI nanoflake arrays as photoactive electrode for photoelectrochemical detection of triphenyl phosphate. *Biosens Bioelectron* **2017**;*92*:61.
234. Yan X, Li HX, Su XG. Review of optical sensors for pesticides. *Trac Trends Anal Chem* **2018**;*103*:1.
235. Watanabe E, Baba K. Highly sensitive quantification of pyrethroid insecticide etofenprox in vegetables with high-performance liquid chromatography and fluorescence detection. *J Chromatogr A* **2015**;*1385*:35.
236. Jafari MT, Saraji M, Sherafatm H. Polypyrrole/montmorillonite nanocomposite as a new solid phase microextraction fiber combined with gas chromatography-corona discharge ion mobility spectrometry for the simultaneous determination of diazinon and fenthion organophosphorus pesticides. *Anal Chim Acta* **2014**;*814*:69.
237. Rodrigues ET, Pardal MA, Salgueiro-Gonzalez N, Muniategui-Lorenzo S, Alpendurada MF. A single-step pesticide extraction and clean-up multi-residue analytical method by selective pressurized liquid extraction followed by on-line solid phase extraction and ultra-high-performance liquid chromatography-tandem mass spectrometry for complex matrices. *J Chromatogr A* **2016**;*1452*:10.
238. Feng K, Zhai MY, Wei YS, Zong MH, Wu H, Han SY. Fabrication of nano/micro-structured electrospun detection card for the detection of pesticide residues. *Foods* **2021**;*10*:889.
239. El-Moghazy AY, Soliman EA, Ibrahim HZ, Marty JL, Istamboulie G, Noguer T. Biosensor based on electrospun blended chitosan-poly (vinyl alcohol) nanofibrous enzymatically sensitized membranes for pirimiphosmethyl detection in olive oil. *Talanta* **2016**;*155*:258.
240. Shao F, Cao JY, Ying Y, Liu Y, Wang D, Guo XY, Wu YP, Wen Y, Yang HF. Preparation of hydrophobic film by electrospinning for rapid SERS detection of trace triazophos. *Sensors* **2020**;*20*:4120.
241. Ji YF, Shi YY, Yang Y, Yang PZ, Wang L, Lu JH, Li JH, Zhou L, Ferronato C, Chovelon JM. Rethinking sulfate radical-based oxidation of nitrophenols: Formation of toxic polynitrophenols, nitrated biphenyls and diphenyl ethers. *J Hazard Mater* **2019**;*361*:152.
242. Wang YA, Li QC, Zhang P, O'Connor D, Varma RS, Yu M, Hou DY. One-pot green synthesis of bimetallic hollow palladium-platinum nanotubes for enhanced catalytic reduction of p-nitrophenol. *J Colloid Interface Sci* **2019**;*539*:161.
243. Gerent GG, Spinelli A. Magnetite-platinum nanoparticles-modified glassy carbon electrode as electrochemical detector for nitrophenol isomers. *J Hazard Mater* **2017**;*330*:105.
244. Wu H, Guo LX, Zhang JL, Miao SL, He CY, Wang B, Wu YQ, Chen ZM. Polyelectrolyte-free layer by layer self-assembled multilayer films of cationic phthalocyanine cobalt(II) and carbon nanotube for the efficient detection of 4-nitrophenol. *Sens Actuators B Chem* **2016**;*230*:359.
245. Han L, Liu SG, Liang JY, Ju YJ, Li NB, Luo HQ. pH-mediated reversible fluorescence nanoswitch based on inner filter effect induced fluorescence quenching for selective and visual detection of 4-nitrophenol. *J Hazard Mater* **2019**;*362*:45.
246. Hu LM, Zhang GS, Wang Q, Wang XJ, Wang P. Effect of microwave heating on persulfate activation for rapid degradation and mineralization of p-nitrophenol. *Acs Sustain Chem Eng* **2019**;*7*:11662.
247. Zhu GD, Tang Q, Huang MH, Yang JM, Xu R, Liu JY. Polyaniline nanoconical array on carbon nanofiber for supersensitive determination of nitrophenol. *Sens Actuators B Chem* **2020**;*320*:128593.
248. Antohe I, Iordache I, Antohe VA, Socol G. A polyaniline/platinum coated fiber optic surface plasmon resonance sensor for picomolar detection of 4-nitrophenol. *Sci Rep* **2021**;*11*:10086.
249. Jadhav SA, Biji P, Panthalingal MK, Krishna CM, Rajkumar S, Joshi DS, Sundaram N. Development of integrated microfluidic platform coupled with surface-enhanced raman spectroscopy for diagnosis of COVID-19. *Med Hypotheses* **2021**;*146*:110356.
250. Xu ZQ, Fan GH, Zheng T, Lin CC, Lin XC, Xie ZH. Aptamer-functionalized metal-organic framework-based electrospun nanofibrous composite coating fiber for specific recognition of ultratrace microcystin in water. *J Chromatogr A* **2021**;*1656*:462542.
251. Yang Y, Zhang ZJ, He YL, Wang ZH, Zhao YB, Sun L. Fabrication of $Ag@TiO_2$ electrospinning nanofibrous felts as SERS substrate for direct and sensitive bacterial detection. *Sens Actuators B Chem* **2018**;*273*:600.
252. Niri AD, Faridi-Majidi R, Saber R, Khosravani M, Adabi M. Electrospun carbon nanofiber-based electrochemical biosensor for the detection of hepatitis B virus. *Biointerface Res Appl Chem* **2019**;*9*:4022.
253. Arshad R, Rhouati A, Hayat A, Nawaz MH, Yameen MA, Mujahid A, Latif U. MIP-based impedimetric sensor for detecting dengue fever biomarker. *Appl Biochem Biotechnol* **2020**;*191*:1384.

Jialing Song is now an enrolled postgraduate student in the College of Environmental Science and Engineering, Donghua University. She has joined the group of professor Manhong Huang since 2017. In 2021, she joined Prof. Li's research group at the Department of Chemistry, National University of Singapore (NUS) through China Scholarship Council. Her main research direction is the nanomaterials, environmental analysis and sensing, and membrane separation technique.

Xuanhao Lin is research fellow of analytical science at National University of Singapore. He is a graduate of National University of Singapore and Shandong University. Prior to joining National University of Singapore, Dr. Lin worked for Hewlett-Package on thermal inkjet printing technology and Institute of Materials Research & Engineering on nanotechnology. His current research interests include chemical sensors, biosensors, and quantum dot bioconjugates for imaging, labeling and sensing, as well as photocatalytic remediation of wastewater.

Liang Ying Ee received his accelerated BSc (Hons.) in Chemistry from the National University of Singapore (NUS) in 2017. He has gained significant industrial work and research experience from Hyflux Pte. Ltd. and Agency for Science, Technology and Research (A*STAR), respectively. In August 2018, he was awarded the NUS Research Scholarship administered by the Singapore Ministry of Education to undertake the PhD program under Prof. Li at NUS. His research area involves the extraction of nanocellulose from agricultural waste and 3D printing of nanocellulosic desalination membrane.

Sam Fong Yau Li is working as a Full Professor at the Department of Chemistry, National University of Singapore (NUS). He received both his BSc (Hons.) and Phd in Chemistry from the Imperial College and DSc from the University of London. Prof. Li has particular expertise and research interest in nanomaterials, 3D printing, environmental analysis and sensing, environmental remediation technologies, capillary electrophoresis, and metabolomics. To date, he has authored/co-authored over 400 papers in peer-reviewed journals (h-index = 56), with numerous papers on the preparation, analysis, and environmental toxicity of nanomaterials that are closely relevant to the reviewed field.

Manhong Huang is working as a Full Professor in the College of Environmental Science and Engineering, Donghua University. She received her PhD in the College of Environmental Science and Engineering, Tongji University, China. In 2011 and 2013, she went to the Department of Environment of Tsinghua University and Geogia Tech West Institute for exchange study, respectively. Prof. Huang has particular expertise and research interest in nanomaterials, environmental analysis and sensing, MFC, and membrane technology. To date, she has authored/co-authored over 100 papers in peer-reviewed journals and many researches have been transformed and applied in the field of practical environment.